

# 1 An evaluation of IASI-NH<sub>3</sub> with ground-based FTIR 2 measurements

3 Enrico Dammers<sup>1</sup>, Mathias Palm<sup>2</sup>, Martin Van Damme<sup>1,3</sup>, Corinne Vigouroux<sup>4</sup>, Dan Smale<sup>5</sup>, Stephanie Conway<sup>6</sup>,  
4 Geoffrey C. Toon<sup>7</sup>, Nicholas Jones<sup>8</sup>, Eric Nussbaumer<sup>9</sup>, Thorsten Warneke<sup>2</sup>, Christof Petri<sup>2</sup>, Lieven Clarisse<sup>3</sup>,  
5 Cathy Clerbaux<sup>3</sup>, Christian Hermans<sup>4</sup>, Erik Lutsch<sup>6</sup>, Kim Strong<sup>6</sup>, James W. Hannigan<sup>9</sup>, Hideaki Nakajima<sup>10</sup>,  
6 Isamu Morino<sup>11</sup>, Beatriz Herrera<sup>12</sup>, Wolfgang Stremme<sup>12</sup>, Michel Grutter<sup>12</sup>, Martijn Schaap<sup>13</sup>, Roy J. Wichink  
7 Kruit<sup>14</sup>, Justus Notholt<sup>2</sup>, Pierre.-F. Coheur<sup>3</sup> and Jan Willem Erisman<sup>1,15</sup>

8 1. Cluster Earth and Climate, Department of Earth Sciences, Vrije Universiteit Amsterdam, Amsterdam, the  
9 Netherlands

10 2. Institut für Umweltphysik, University of Bremen, Bremen, Germany

11 3. Spectroscopie de l'Atmosphère, Service de Chimie Quantique et Photophysique, Université Libre de Bruxelles  
12 (ULB), Brussels, Belgium

13 4. Royal Belgian Institute for Space Aeronomy (BIRA-IASB), Brussels, Belgium

14 5. National Institute of Water and Atmosphere, Lauder, New Zealand

15 6. University of Toronto, Toronto, Ontario, Canada

16 7. Jet Propulsion Laboratory, California Institute of Technology, Pasadena

17 8. University of Wollongong, Wollongong, Australia

18 9. NCAR, Boulder, Colorado, United States

19 10. Atmospheric Environment Division, National Institute for Environmental Studies (NIES), Japan

20 11. National Institute for Environmental Studies, 16-2 Onogawa, Tsukuba, Ibaraki, 305-8506, Japan

21 12. Centro de Ciencias de la Atmosfera, Universidad Nacional Autonoma de Mexico, Mexico City, Mexico

22 13. TNO Built Environment and Geosciences, Department of Air Quality and Climate, Utrecht, the Netherlands

23 14. National Institute for Public Health and the Environment (RIVM), Bilthoven, the Netherlands

24 15. Louis Bolk Institute, Driebergen, the Netherlands

25

26 *Correspondence to:* E. Dammers (e.dammers@vu.nl)

27 **Abstract.** Global distributions of atmospheric ammonia (NH<sub>3</sub>) measured with satellite instruments such as the  
28 Infrared Atmospheric Sounding Interferometer (IASI) contain valuable information on NH<sub>3</sub> concentrations and  
29 variability in regions not yet covered by ground based instruments. Due to their large spatial coverage and (bi-)  
30 daily overpasses, the satellite observations have the potential to increase our knowledge of the distribution of  
31 NH<sub>3</sub> emissions, and associated seasonal cycles. However the observations remain poorly validated, with only a  
32 handful of available studies often using only surface measurements without any vertical information. In this  
33 study, we present the first validation of the IASI-NH<sub>3</sub> product using ground-based Fourier Transform InfraRed  
34 (FTIR) observations. Using a recently developed consistent retrieval strategy, NH<sub>3</sub> concentration profiles have  
35 been retrieved using observations from nine Network for the Detection of Atmospheric Composition Change  
36 (NDACC) stations around the world between 2008- 2015. We demonstrate the importance of strict spatio-  
37 temporal collocation criteria for the comparison. Large differences in the regression results are observed for  
38 changing intervals of spatial criteria, mostly due to terrain characteristics and the short lifetime of NH<sub>3</sub> in the  
39 atmosphere. The seasonal variations of both datasets are consistent for most sites. Correlations are found to be  
40 high at sites in areas with considerable NH<sub>3</sub> levels, whereas correlations are lower at sites with low atmospheric  
41 NH<sub>3</sub> levels close to the detection limit of the IASI instrument. A combination of the observations from all sites  
42 ( $N_{\text{obs}} = 547$ ) give a MRD of  $-32.4 \pm (56.3) \%$ , a correlation  $r$  of 0.8 with a slope of 0.73. These results give an  
43 improved estimate of the IASI-NH<sub>3</sub> product performance compared to the previous upper bound estimates (-  
44 50% - +100%).

## 45 1. Introduction

46  
47 Humankind has increased the global emissions of reactive nitrogen to an unprecedented level (Holland et al.,  
48 1999; Rockström et al., 2009). The current global emissions of reactive nitrogen are estimated to be a factor four  
49 larger than pre-industrial levels (Fowler et al., 2013). Consequently atmospheric deposition of reactive nitrogen  
50 to ecosystems has substantially increased as well (Rodhe et al., 2002; Dentener et al., 2006). Ammonia ( $\text{NH}_3$ )  
51 emissions play a major role in this deposition with a total emission of 49.3Tg in 2008 (Emission Database for  
52 Global Atmospheric Research (EDGAR), 2011). Although  $\text{NH}_3$  emissions are predominantly from agriculture in  
53 the Northern Hemisphere, wildfires also play a role, with biomass burning contributing up to 8% of the global  
54 emission budget (Sutton et al., 2013).  $\text{NH}_3$  has been shown to be a major factor in the acidification and  
55 eutrophication of soil and water bodies, which threatens biodiversity in vulnerable ecosystems (Bobbink et al.,  
56 2010; Erisman et al., 2008, 2011). Through reactions with sulphuric and nitric acid,  $\text{NH}_3$  also contributes to the  
57 formation of particulate matter which is associated with adverse health effects (Pope et al., 2009). Particulate  
58 ammonium salts contribute largely to aerosol loads over continental regions (Schaap et al., 2004). Through its  
59 role in aerosol formation,  $\text{NH}_3$  also has an impact on global climate change as hygroscopic ammonium salts are  
60 of importance for the aerosol climate effect and thus the global radiance budget (Adams et al., 2001).  
61 Furthermore increased  $\text{NH}_3$  concentrations in the soil also enhance the emission of nitrous oxide ( $\text{N}_2\text{O}$ ) which is  
62 an important greenhouse gas and an ozone-depleting substance (Ravishankara et al., 2009). Finally nitrogen  
63 availability is a key factor for the fixation of carbon dioxide ( $\text{CO}_2$ ) and thus it is an important factor in climate  
64 change.

65 Despite the fact that  $\text{NH}_3$  at its current levels is a major threat to the environment and human health, relatively  
66 little is known about its total budget and global distribution (Sutton et al., 2013; Erisman et al., 2007). Surface  
67 observations are sparse and mainly available for north-western Europe, the United States and China (Van  
68 Damme et al., 2015a). At the available sites, in situ measurements are mostly performed with relatively poor  
69 temporal resolution due to the high costs of performing reliable  $\text{NH}_3$  measurements with high temporal  
70 resolution. These measurements of  $\text{NH}_3$  are also hampered by sampling artefacts caused by the reactivity of  $\text{NH}_3$   
71 and the evaporation of ammonium nitrate (Slanina et al., 2001; von Bobruzki et al., 2010; Puchalski et al.,  
72 2011). As the lifetime of atmospheric  $\text{NH}_3$  is rather short, on the order of hours to a few days, due to efficient  
73 deposition and fast conversion to particulate matter, the existing surface measurements are not sufficient to  
74 estimate global emissions without inducing large errors. The lack of vertical profile information further hampers  
75 the quantification of the budget, with only a few reported airborne measurements (Nowak et al., 2007, 2010,  
76 Leen et al., 2013, Whitburn et al., 2015).

77 Advanced IR-sounders such as the Infrared Atmospheric Sounding Interferometer (IASI), the Tropospheric  
78 Emission Spectrometer (TES), and the Cross-track Infrared Sounder (CrIS) enable retrievals of atmospheric  
79  $\text{NH}_3$  (Beer et al., 2008; Coheur et al., 2009; Clarisse et al., 2009; Shephard et al., 2011, 2015a). The availability  
80 of satellite retrievals provide a means to consistently monitor global  $\text{NH}_3$  distributions. Global distributions  
81 derived from IASI and TES observations have shown high  $\text{NH}_3$  levels in regions not covered by ground-based  
82 data. In this way, more insight was gained into known and unknown  $\text{NH}_3$  sources worldwide including biomass  
83 burning, industry and agricultural areas. Hence, satellite observations have the potential to improve our

84 knowledge of the distribution of global emissions and their seasonal variation due to their large spatial coverage  
85 and (bi-) daily observations (Zhu et al., 2013; Van Damme et al., 2014b, 2015b; Whitburn et al., 2015; Luo et  
86 al., 2015). However, the satellite observations remain poorly validated with only a few dedicated campaigns  
87 performed with limited spatial, vertical or temporal coverage (Van Damme et al., 2015a; Shephard et al., 2015b,  
88 Sun et al., 2015).

89 Only a few studies have explored the quality of the IASI-NH<sub>3</sub> product. A first evaluation of the IASI  
90 observations was made over Europe using the LOTOS-EUROS model and has shown the respective consistency  
91 of the measurements and simulations (Van Damme et al., 2014b). A first comparison using ground-based and  
92 airborne measurements to validate the IASI-NH<sub>3</sub> data set were made in Van Damme et al. (2015a). They  
93 confirmed consistency between the IASI-NH<sub>3</sub> data set and the available ground-based observations and showed  
94 promising results for validation by using independent airborne data from the CalNex campaign. Nevertheless,  
95 that study was limited by the availability of independent measurements and suffered from representativeness  
96 issues for the satellite observations when comparing to surface concentration measurements. One of the key  
97 conclusions was the need for vertical profiles (e.g. ground-based remote sensing products or upper-air in situ  
98 measurements to compare similar quantities). Recently, Dammers et al. (2015) developed a retrieval  
99 methodology for Fourier Transform Infrared Spectroscopy (FTIR) instruments to obtain remotely sensed  
100 measurements of NH<sub>3</sub> and demonstrated the retrieval characteristics for four sites located in agricultural and  
101 remote areas. Here we explore the use of NH<sub>3</sub> total columns obtained with ground based FTIR at nine stations  
102 with a range of NH<sub>3</sub> pollution levels to validate the IASI-NH<sub>3</sub> satellite product by Van Damme (2014a).

103 First, we concisely describe the ground based FTIR retrieval and IASI-NH<sub>3</sub> product datasets in Sections 2.1 and  
104 2.2. Next we describe the methodology of the comparison in Section 2.3 followed by the presentation of the  
105 results in Section 3, which are then summarized and discussed in Section 4.

106

107 **2. Description of the satellite and FTIR data sets and validation methodology**

108 **2.1 IASI-NH<sub>3</sub> product**

109 The first global NH<sub>3</sub> distribution was obtained by a conventional retrieval method applied to IASI spectra  
110 (Clarisse et al., 2009), followed by an in depth case study, using a more sophisticated algorithm, of the  
111 sounder's capabilities depending on the thermal contrast (defined in Van Damme et al. (2014a) as the  
112 temperature differences between the Earth surface and the atmosphere at 1.5 km altitude, Clarisse et al., 2010).  
113 In this study we use the NH<sub>3</sub> product developed by Van Damme et al. (2014a). Their product is based on the  
114 calculation of a dimensionless spectral index (Hyperspectral Range Index: HRI), which is a quantity  
115 representative of the amount of NH<sub>3</sub> in the total atmospheric column. This HRI is then converted into NH<sub>3</sub> total  
116 columns using look-up-tables based on numerous forward simulations for various atmospheric conditions.  
117 These look-up-tables relate the HRI and the thermal contrast to a total column of NH<sub>3</sub> (Van Damme et al.,  
118 2014a). The product includes an error characterization of the retrieved column based on errors in the thermal  
119 contrast and HRI. Important advantages of this method over the method by Clarisse (2009) is the relatively  
120 small computational cost, the improved detection limit and the ability to identify smaller emission sources and  
121 transport patterns above the sea. One of the limitations of this method is the use of only two NH<sub>3</sub> vertical  
122 profiles: a "source profile" for land cases and a "transported profile" for sea cases (Illustrated in Van Damme et  
123 al., 2014a, fig. 3). Another limitation of the product is that it does not allow the calculation of an averaging  
124 kernel to account for the vertical sensitivity of the instrument sounding to different layers in the atmosphere. In  
125 this paper we will use NH<sub>3</sub> total columns retrieved from the IASI-A instrument (aboard of the MetOp-A  
126 platform) morning overpass (AM) observations (i.e. 09:30 local time at the equator during overpass) which have  
127 a circular footprint of 12 km diameter at nadir and an ellipsoid shaped footprint of up to 20 km x 39 km at the  
128 outermost angles. We will use observations from January 1<sup>st</sup> 2008 to December 31<sup>st</sup> 2014. Figure 1 shows the  
129 mean IASI-NH<sub>3</sub> total column distribution (all observations gridded to a 0.1° x 0.1° grid) using observations  
130 above land for the years 2008-2014. The mean columns are obtained through a weighting with the relative error  
131 (see Van Damme et al., 2014). The bottom left inset shows the corresponding relative error.

132

133

## 134 2.2 FTIR- NH<sub>3</sub> retrieval

135

136 The FTIR-NH<sub>3</sub> retrieval methodology used here is described in detail in Dammers et al. (2015) and a summary  
137 is given here. The retrieval is based on the use of two spectral micro-windows, which contain strong individual  
138 NH<sub>3</sub> absorption lines. The two spectral windows [930.32-931.32 cm<sup>-1</sup>, MW1] and [962.70-970.00 cm<sup>-1</sup>, MW2]  
139 or the wider version for regions with very low concentrations [929.40-931.40 cm<sup>-1</sup>, MW1 Wide] and [962.10-  
140 970.00 cm<sup>-1</sup>, MW2 Wide] are fitted using SFIT4 (Pougatchev et al., 1995; Hase et al., 2004, 2006) or a similar  
141 retrieval algorithm (Hase et al, 1999) based on the optimal estimation method (Rodgers et al., 2000) to retrieve  
142 the volume mixing ratios (in ppbv) and total columns of NH<sub>3</sub> (in molecules cm<sup>-2</sup>). Major interfering species in  
143 these windows include H<sub>2</sub>O, CO<sub>2</sub> and O<sub>3</sub>. Minor interfering species are N<sub>2</sub>O, HNO<sub>3</sub>, CFC-12 and SF<sub>6</sub>. For the  
144 line spectroscopy, the HITRAN 2012 (Rothman et al., 2013) database is used with a few adjustments for CO<sub>2</sub>  
145 (ATMOS, Brown et al., 1996), and sets of pseudo-lines generated by NASA-JPL (G.C. Toon) are used for the  
146 broad absorptions by heavy molecules (i.e. CFC-12, SF<sub>6</sub>). The *a-priori* profiles of NH<sub>3</sub> are based on balloon  
147 measurements (Toon et al., 1999) and scaled to fit common surface concentrations at each of the sites. An  
148 exception is made for the a-priori profile at Reunion Island where a modelled profile from the MOZART model  
149 is used (Louisa Emmons, personal communication, 2014). There, the profile peaks at a height of 4-5 km, as NH<sub>3</sub>  
150 are expected to be due to transport of biomass burning emissions on the island and Madagascar. For all stations,  
151 the *a-priori* profiles for interfering species are taken from the Whole Atmosphere Community Climate Model  
152 (WACCM, Chang et al., 2008). Errors in the retrieval are typically ~30% (Dammers et al., 2015), which are  
153 mostly due to uncertainties in the spectroscopy in the line intensities of NH<sub>3</sub> and the temperature and pressure  
154 broadening coefficients (HITRAN 2012).

155

156 An effort has been made to gather observations from most of the station part of the Network for the Detection of  
157 Atmospheric Composition Change (NDACC) which have obtained relevant solar spectra between 1<sup>st</sup> of Jan  
158 2008 and 31<sup>st</sup> of Dec 2014. We excluded stations which have only retrieved or are believed to have, NH<sub>3</sub> total  
159 columns smaller than 5x10<sup>15</sup> (molecules cm<sup>-2</sup>) during the study interval (i.e. Arctic and Antarctic and other  
160 stations with concentrations below the expected limits of the IASI-NH<sub>3</sub> product, at best ~5x10<sup>15</sup> for observations  
161 with high thermal contrast). Figure 1 shows the positions of the FTIR stations used in this study. The retrieved  
162 NH<sub>3</sub> total columns (molecules cm<sup>-2</sup>) for each of the stations are shown in Figure 2. The number of available  
163 observations per station varies as does the range in total columns with high values of ~100x10<sup>15</sup> (molecules cm<sup>-2</sup>)  
164 observed at Bremen and low values of about 1x10<sup>15</sup> (molecules cm<sup>-2</sup>) at St Denis Reunion. The following  
165 provides a short description of each of the sites used in this study and retrieved NH<sub>3</sub> columns (molecules cm<sup>-2</sup>).  
166 Additionally, a short summary can be found in Table 1:

167 The **Bremen** site operated on the university campus by the University of Bremen in the northern part of the city  
168 (Velazco et al., 2007). Bremen is located in the northwest of Germany, which is characterized by intensive  
169 agriculture. It is most suitable for comparisons with IASI given the very high observed concentrations (Fig. 2,  
170 blue) and flat geography surrounding the station. NH<sub>3</sub> sources near the measurement station include manure  
171 application to fields, livestock housing and exhaust emissions of local traffic. The retrieved NH<sub>3</sub> total columns  
172 peak in spring due to manure application and show an increase in summer due to increased volatilization of NH<sub>3</sub>  
173 from livestock housing and fields when temperatures increase during summer.

174 The **Toronto** site (Wiacek et al., 2007) is located on the campus of the University of Toronto, Canada. The city  
175 is next to Lake Ontario with few sources to the south. NH<sub>3</sub> sources are mainly due to agriculture as well as local  
176 traffic in the city. Occasionally, NH<sub>3</sub> in smoke plumes from major boreal fires to the north and west of the city  
177 can be observed (Lutsch et al., 2016). The retrieved columns (Fig. 2, green) show increased values during  
178 summers as well as peaks in spring.

179 The **Boulder** observation site is located at the NCAR Foothills Lab in Boulder, Colorado, United States of  
180 America, about 60 km northwest of the large metropolitan Denver area. It is located at 1.6 km a.s.l. on the  
181 generally dry Colorado Plateau. Directly to the west are the foothills of the Rocky Mountain range and to the  
182 east are rural grasslands, farming and ranching facilities. Among them are large cattle feed lots to the northeast  
183 near Greeley approximately 90 km distant. The area is subject to occasional seasonal local forest fires and also  
184 occasionally sees plumes from fires as distant as Washington or California. The retrieved columns (Fig. 2, grey)  
185 show the largest increase during summers.

186 The **Tsukuba** site (Ohyama et al., 2009) is located at the National Institute for Environmental Studies (NIES),  
187 in Japan. The region is a mixture of residential and rural zones with mountains to the north. NH<sub>3</sub> sources near  
188 the measurement site include manure and fertilizer applications and exhaust emissions of local traffic in the  
189 surrounding city with a large part originating from the from the Tokyo metropolitan area. The retrieved columns  
190 (Fig 2, red) show a general increase during the summers due to increased volatilization rates.

191 The **Pasadena** site lies on the Northern edge of the Los Angeles conurbation in the United States of America, at  
192 the foot of the San Gabriel mountains which rise steeply to the north to over 1.5 km altitude within 5 km  
193 distance. Local sources of NH<sub>3</sub> include traffic, livestock, and occasional fires. FTIR observations typically take  
194 place around local noon to avoid solar obstruction by nearby buildings and morning stratus cloud that is  
195 common May-July. The highest retrieved columns (Fig.2, cyan) are observed during the summers.

196 The **Mexico City** site is located on the campus of the National Autonomous University of Mexico (UNAM) at  
197 2280 m a.s.l., south of the metropolitan area. Surface NH<sub>3</sub> concentrations were measured by active open-path  
198 FTIR during 2003 with typical values between 10 - 40 ppb (Moya et al. 2004). The megacity is host to more  
199 than 22 million inhabitants, over 5 million motor vehicles and a wide variety of industrial activities. Low  
200 ventilation during night and morning causes an effective accumulation of the NH<sub>3</sub> and other pollutants in  
201 Mexico City, which is located in a flat basin surrounded by mountains. The concentration and vertical  
202 distribution of pollutants are dominated by the large emissions and the dynamics of the boundary layer which is  
203 on average 1.5 km height during the IASI morning overpass (Stremme et al., 2009, 2013). The retrieved  
204 columns (Fig.2, orange) show an increase during the summers as well as a large daily variation.

205 The measurement site on the university campus of **St.-Denis** (Senten et al., 2008) is located on the remote  
206 Reunion Island in the Indian Ocean. Observed NH<sub>3</sub> columns (Fig. 2, purple) are usually low due to the lack of  
207 major sources nearby the site but increases are observed during the fire season (Sept.-Nov.) with possible fire  
208 plumes originating from Madagascar, as already observed in another study involving short-lived species  
209 (Vigouroux et al., 2009). Local NH<sub>3</sub> emissions include fertilizer applied for sugar cane production and local  
210 biomass burning.

211 The **Wollongong** site is located on the campus of the University of Wollongong. The city of Wollongong is on  
212 the south east coast of Australia with the University only about 2.5 km from the ocean. The measurement site is  
213 also influenced by a 400m escarpment 1 km to the West, and the city of Sydney 60 km to the north. NH<sub>3</sub>

214 sources come mainly from city traffic, as well as seasonal forest fires that can produce locally high amounts of  
215 smoke and subsequent NH<sub>3</sub> emissions (Paton-Walsh et al., 2005). The retrieved columns (Fig.2, brown) peak  
216 during the summer season due to the higher temperatures and seasonal forest fires.  
217 The **Lauder** (Morgenstern et al., 2012) National Institute of Water and Atmospheric Research (NIWA) station  
218 in Central Otago, New Zealand, is located in a hilly region with NH<sub>3</sub> emissions in the valley surrounding the  
219 station mostly due to livestock grazing and fertilizer application. The observed columns (Fig. 2, black) show a  
220 general increase during summers due to increased volatilization rates.  
221  
222

## 223 **2.3 FTIR and satellite comparison methodology**

### 224 **2.3.1 Co-location & data criteria**

225

226 NH<sub>3</sub> is highly variable in time and space which complicates the comparison between the IASI and FTIR  
227 observations. Therefore collocation criteria were developed to investigate and mitigate the effect of the spatial  
228 and temporal differences between the FTIR and IASI observations on their correlation. So far, there is no model  
229 to describe the representativeness of a site for the region so a simple criterion was initially derived by analyzing  
230 the terrain around each site and comparing the correlation of the IASI and FTIR observations for multiple time  
231 and spatial differences to find the best correlation. To illustrate the differences between the representativeness of  
232 the sites we take the stations at Bremen, Lauder and Wollongong as examples. Around Bremen the terrain is flat  
233 with high reported NH<sub>3</sub> emissions (Kuenen et al., 2014) in the region surrounding the city. In contrast, Lauder is  
234 located in a hilly region with low NH<sub>3</sub> emissions mostly due to local livestock grazing and fertilizer application  
235 in the surrounding valleys (EDGAR, 2011). Owing to the flat terrain, the region around Bremen should, in  
236 principle, have more homogeneous concentrations than Lauder. A more extreme case for geographical  
237 inhomogeneity is Wollongong. Wollongong is located at the coast near a 400m escarpment without major  
238 nearby NH<sub>3</sub> sources. Hence increasing distances between the satellite measurement pixel center and the station  
239 may negatively impact the comparison due to the short lifetime of NH<sub>3</sub>, and the limitation on transport of NH<sub>3</sub>  
240 to the site by the terrain (i.e. representativeness problems). Because no uniform criterion was found that would  
241 enable a good comparison for all stations, multiple criteria with a maximum difference of between 10 km and 50  
242 km will be used to analyze the optimal setting for each of the sites. Vertical sampling differences are not taken  
243 into consideration in this study however the IASI selection criterion on the thermal contrast is conservative  
244 and only those measurements for which IASI has a good sensitivity to surface concentrations are selected.

245

#### 246 **Topography**

247 Any hill or mountain range located between the satellite pixel and the FTIR station may inhibit transport and  
248 decrease their comparability. To account for the topography we only used observations that have at maximum  
249 an altitude difference of 300 m (in) between the location of the FTIR and the IASI pixel position. The 300 m  
250 criterion was chosen based on tests using the FTIR and satellite observations from Lauder. For the calculation of  
251 the height differences we used the Space Shuttle Radar Topography Mission Global product at 3 arc second  
252 resolution (SRTMGL3, Farr et al., 2007).

253

#### 254 **Temporal variation**

255 NH<sub>3</sub> concentrations can vary considerably during the day, with lifetimes as short as a few hours not being  
256 uncommon (Dentener and Crutzen, 1994; Bleeker et al., 2009). The variability of the concentrations mainly  
257 arises from the variability in emission strengths as influenced by agricultural practices, meteorological, and  
258 atmospheric conditions such as temperature, precipitation, wind speed and direction, the development of the  
259 boundary layer (which is important as the IASI satellite observations take place around 9.30 local time and thus  
260 the boundary layer has not always been fully established), pollution level, and deposition rates. To minimize the  
261 effects of this variability on the comparability of the IASI and FTIR observations, satellite observations with a  
262 time difference to FTIR observation of no more than 90 minutes were used.

263



264 **Product error**

265 The error of the IASI-NH<sub>3</sub> columns derives from errors on the HRI and the thermal contrast (Van Damme et al.,  
266 2014a). Applying relative error filters of 50, 75 and 100% showed that mostly lower concentrations are removed  
267 from the comparison. Consequently, introducing any criteria based on the associated (relative) error will bias  
268 any comparison with FTIR columns towards the higher IASI total columns. Therefore, we decided not to filter  
269 based on the relative error as it skews the range of NH<sub>3</sub> column totals.

270  
271 **Meteorological factors**

272 The lowest detectable total column of the retrieval depends on the thermal contrast of the atmosphere (Van  
273 Damme et al., 2014a). For example, the retrieval has a minimum detectable NH<sub>3</sub> column of around  $5 \times 10^{15}$   
274 molecules cm<sup>-2</sup> at a thermal contrast of about 12 Kelvin (K) for columns using the “transported” profile. A  
275 thermal contrast of 12 K is chosen as the threshold to ensure the quality of the IASI observations, which  
276 represents a lapse rate of around 8K/km altitude, near standard atmospheric conditions. We excluded data for  
277 T<sub>skin</sub> temperatures below 275.15 K to introduce a basic filter for snow cover and conditions with frozen soils.  
278 The T<sub>skin</sub> temperatures are obtained from the IASI L2 temperature profiles which have an uncertainty of ~2 K at  
279 the surface (August et al., 2012). Finally, only IASI observations with a cloud cover below 10% are used.

280  
281 The complete list of selection criteria is summarized in Table 2.

282  
283 **Quality of the FTIR observations**

284 No filters were applied to maximize the number of observations usable in the comparison. The resolution and  
285 detection limit of the FTIR instruments is usually better than that of the IASI instrument, leading to retrieved  
286 columns with, in principle, less uncertainty. Overall the FTIR retrievals show an error of ~30% or less with the  
287 largest errors due to the spectroscopic parameters (Dammers et al., 2015). While artefacts are possible in the  
288 data we did not investigate for specific artefacts and possible impacts.

289  
290  
291 **2.3.2 Application of averaging kernels**

292 When performing a direct comparison between two remote sensing retrievals, one should take into account the  
293 vertical sensitivity and the influence of a-priori profiles of both methods. One method to remove the influence of  
294 the a-priori profile and the vertical sensitivity is the application of the averaging kernels of both retrievals to the  
295 retrieved profiles of both products. The IASI-NH<sub>3</sub> HRI-based product scheme however, does not produce  
296 averaging kernels thus it is not possible to account for the vertical sensitivity of the satellite retrieval. The effect  
297 of the lack of the satellite averaging kernel is hard to predict, so the satellite vertical sensitivity is only taken into  
298 account through the selection criterion on the thermal contrast. Nonetheless following the method described in  
299 Rodgers and Connor (2003), the FTIR averaging kernel **A** is applied to the IASI profile  $x_{sat}$  to account for the  
300 effects of the a-priori information and vertical sensitivity of the FTIR retrieval (the assumed profiles, called  
301 “land” and “sea” are described in Van Damme et al., 2014a). The IASI profiles are not fully retrieved profiles  
302 but fixed shape profiles used as an assumption in the IASI retrieval, see Van Damme et al., 2015a. These fixed  
303 profiles are used for scaling purposes to be able to account for the FTIR averaging kernel. A total column

304 averaging kernel could be used instead, but in principle is similar to the procedure described here. The IASI  
 305 profile is first mapped to the altitude grid of the FTIR profile by using interpolation, forming  $x_{sat}^{mapped}$ . Applying  
 306 Eqn. (1), the smoothed IASI profile  $\hat{x}_{sat}$  is calculated indicating what the FTIR would retrieve when observing  
 307 the satellite profile, which is then used to compute a total column. This profile can then be compared with the  
 308 FTIR profile.

$$309 \quad \hat{x}_{sat} = x_{ftir}^{apriori} + A(x_{sat}^{mapped} - x_{ftir}^{apriori}) \quad (1)$$

310 After the application of the averaging kernel, for each FTIR observation, all satellite observations meeting the  
 311 coincident criteria are averaged into a single mean total column value to be compared with the FTIR value. If  
 312 multiple FTIR observations match a single satellite overpass, taking into account the maximum time difference,  
 313 the FTIR observations are also averaged into a single mean total column value.

314

### 315 **3. Results**

#### 316 **3.1 The influence of spatial differences between observations**

317

318 Following the approach of Irie et al. (2012) we will first show the correlation  $r$ , the slope as well as the mean  
 319 relative difference (MRD) and the mean absolute difference (MAD) between satellite (y-axis) and FTIR NH<sub>3</sub>  
 320 total columns (x-axis) for each of the sites, as a function of the maximum allowable spatial difference between  
 321 the observations (xdiff). The relative difference (RD) is defined here as,

322

$$323 \quad RD = \frac{(IASI \text{ column} - FTIR \text{ column}) \times 100}{FTIR \text{ column}} \quad (2)$$

324

325 A maximum relative difference of 200% was used to remove extreme outliers from the data, typically  
 326 observations under wintertime conditions. The left side of Figure 3 shows the correlation coefficients (blue  
 327 lines) and slope (red lines) for a selection of sites as a function of xdiff using a maximum allowed sampling time  
 328 difference of 90 minutes. The right side of Figure 3 shows the MRD and MAD between the satellite and FTIR  
 329 observations as a function of xdiff. The numbers on the bottom of each of the subfigures show the number of  
 330 observations used in the comparison. The values in bold beside the title of each subplot give the mean  
 331 concentrations of the IASI and FTIR observations. The bars indicate the standard deviation of the slope (left  
 332 side figures) and the relative and absolute differences (right side figures).

333

334 For most stations an increasing xdiff (Figure 3) means a decreasing correlation (blue lines) and a changing slope  
 335 (either decreasing or increasing with distance, red lines). This can be explained by the local character and high  
 336 variation of NH<sub>3</sub> emissions/concentration in combination with the locations of the stations. Moving further away  
 337 from a source will then generally decrease the relation between the concentration in the air and the emission  
 338 source. The same is true for satellite observations of the air concentrations, which have a large footprint  
 339 compared to the local character of a point measurement (FTIR) and the emissions. The steepness of this  
 340 decrease (or increase) tells us something about the local variation in NH<sub>3</sub> concentrations, which can be large for

341 sites near heterogeneous emission sources or in cases with low transport/turbulence and thus overall relatively  
342 low mixing.

343

344 Overall the highest correlations are seen at the Bremen site, which can partially be explained by the overall high  
345 number of observations with high concentrations (more than  $15\text{-}20 \times 10^{15}$  molecules  $\text{cm}^{-2}$ ) which generally favours  
346 the correlations. The mean column totals as well as the MRD and MAD do not change much except for the  
347 smallest xdiff criteria. The larger changes for observations within 15 km are probably due to the smaller number  
348 of observations (which follows from the relatively few IASI observations directly above or near the stations).  
349 The results show an underestimation of observed columns by IASI with the “all stations” slopes in between  
350  $\sim 0.6\text{-}0.8$ . The stations with a lower mean FTIR column totals, such as Toronto and Boulder (as well as  
351 Pasadena, Mexico City, and Lauder shown in the Appendix Figure A1) show lower correlations with most  
352 having slopes below one. The correlations decreasing with mean column totals point towards the product  
353 detection limits of the IASI- $\text{NH}_3$  product. The Toronto site has lower correlation coefficients for the smallest  
354 xdiffs, but this seems to be due to the large drop in number of observations for a xdiff of  $<15$  km. For higher  
355 xdiff criteria the correlations of the Toronto site shows results similar to Bremen. The observations at Boulder  
356 also show large differences when including more observations further away from the station. This can be  
357 explained by the land use surrounding the Boulder site. Immediately west of the measurement site is a mountain  
358 range which together with our elevation filter leads to rejection of the observations to the west. To the northeast  
359 there are some major farming areas surrounding the river banks. Correlations do increase with a decreasing  
360 xdiff, suggesting that IASI is able to resolve the large gradients in the  $\text{NH}_3$  concentrations near the site.

361

362 From the correlation analysis as function of spatial coincidence, we conclude that a xdiff value of 25 km is  
363 recommended to make a fair comparison between IASI- $\text{NH}_3$  and FTIR. Any criteria smaller than 15 km greatly  
364 reduces the number of observations and statistics. xdiff beyond 25 km further decrease the correlations for the  
365 combined set. From this point onward a xdiff value of 25 km will be used.

366

### 367 **3.2 Comparison of FTIR and IASI $\text{NH}_3$ data**

368 Observations from multiple years are used to show the coincident seasonal variability of the FTIR and IASI-  
369  $\text{NH}_3$  products for each of the sites (Figure 4, FTIR: blue, IASI: red). Observations are grouped together into a  
370 typical year as there are insufficient collocated observations to show an inter-annual time series. Note the  
371 different scales on the y-axis. Similar seasonal cycles are clearly observed in both datasets for most stations.  
372 Enhanced concentrations in spring are observed for Bremen and Toronto as well as Boulder due to manure  
373 application. Most of the sites show an increase of  $\text{NH}_3$  during the summer months which is likely due to the  
374 increased volatilization of  $\text{NH}_3$  as an effect of higher temperatures. Fire events that were earlier captured by  
375 FTIR at St.-Denis in November, as well as in the IASI data, are not observed in the collocated sets, which is due  
376 to a lack of coincident observations. Furthermore, there is a lack of observations in wintertime for most of the  
377 stations either due to low thermal contrast or due to overcast conditions. Tsukuba has observations above the  
378 detection limit but only one year of infrequent observations which is insufficient to show an entirely clear  
379 seasonal cycle. A similar thing can be said for Pasadena where the number of coincident observations are too

380 few to make meaningful conclusions about the seasonal cycle. In conclusion, IASI reflects similar pollution  
381 levels and seasonal cycles as deduced from the FTIR observations.

382

383 Figure 5 and 6 show a direct comparison of the FTIR and IASI  $\text{NH}_3$  total columns for each station as well as a  
384 combination of all the observations. Correlations, number of observations and slope are shown in the figures.  
385 The MRD and these statistics are also summarized in Table 3. The comparison shows a variety of results. As  
386 before, of all 9 stations Bremen shows the best correlation with a coefficient of determination of  $r = 0.83$  and a  
387 slope of 0.60. The intercept is not fixed at zero. The stations with overall lower observed total columns (less  
388 than  $10 \times 10^{15}$  molecules  $\text{cm}^{-2}$ ) show lower correlations. Stations with intermediate concentrations like Toronto  
389 and Boulder show correlations  $r = \sim 0.7-0.8$ . The figure also shows the relatively low number of high  
390 observations for both the FTIR and IASI values as a result of the relatively few FTIR observations during  
391 events. The few outliers can have a disproportional effect on the slope as most of the lower observations are less  
392 accurate due to the detection limits of the instruments. Overall most stations, except St.-Denis and Boulder and  
393 Mexico City, indicate an underestimation by IASI of the FTIR columns ranging from 10-50%. The mean  
394 relative differences for most stations are negative with most showing values in between  $-22.5 \pm (54.0) \%$  for  
395 Bremen down to a  $-61.3 \pm (78.7) \%$  for St.-Denis. The bias shows some dependence on the total columns with  
396 the underestimation being higher at stations with high mean total columns and lower at stations with low mean  
397 total columns. An exception to this are stations with the lowest mean total columns (i.e. St.-Denis and  
398 Wollongong). The differences at St.-Denis might be explained by the fact that most IASI observations are  
399 positioned above water due to restrictions for terrain height differences. A similar thing can be said for  
400 Wollongong which is situated on the coast with hills directly to the inland. Most observations are on the border  
401 of water and land which might introduce errors in the retrieval. The combination of all observations gives a  
402 MRD of  $-32.4 \pm (56.3) \%$ .

403

#### 404 **4. Discussion and conclusions**

405

406 Recent satellite products enable the global monitoring of atmospheric concentrations of  $\text{NH}_3$ . Unfortunately, the  
407 validation of the satellite products of IASI (Van Damme et al., 2014a), TES (Shephard et al., 2011) and CrIS  
408 (Shephard et al., 2015a) is very limited and, so far, only based on sparse in-situ and airborne studies. Dammers et  
409 al. (2015) presented FTIR total column measurements of  $\text{NH}_3$  at several places around the world and demonstrated  
410 that these data can provide information about the temporal variation of the column concentrations, which are more  
411 suitable for validation than ground-level concentrations. Ground-based remote sensing instruments have a long  
412 history for validation of satellite products. FTIR observations are already commonly used for the validation of  
413 many satellite products, including carbon monoxide ( $\text{CO}$ ), methane ( $\text{CH}_4$ ) and nitrous oxide ( $\text{N}_2\text{O}$ ) (Wood et al.,  
414 2002; Griesfeller et al., 2006; Dils et al., 2006; Kerzenmacher et al., 2012). Furthermore, MAX-DOAS systems  
415 are used for the validation of retrievals for reactive gases (e.g. Irie et al., 2012), whereas AERONET is widely  
416 used to validate satellite-derived aerosol optical depth (e.g. Schaap et al., 2008). The comparison between FTIR  
417 and IASI  $\text{NH}_3$  column reported here can be seen as a first step in the validation of  $\text{NH}_3$  satellite products.

418

419 In this study, we collected FTIR measurements from nine locations around the world and followed the retrieval  
420 described by Dammers et al. (2015). The resulting datasets were used to quantify the bias and evaluate the  
421 seasonal variability in the IASI-NH<sub>3</sub> product. Furthermore, we assessed the collocation criteria for the satellite  
422 evaluation. Additional selection criteria based on thermal contrast, surface temperature, cloud cover and  
423 elevation differences between observations, were applied to ensure the quality of the IASI-NH<sub>3</sub> observations.  
424 The FTIR averaging kernels were applied to the satellite profiles to account for the vertical sensitivity of the  
425 FTIR and the influence of the a-priori profiles.

426

427 To optimally compare the satellite product to the FTIR observations it is best to reduce the spatial collocation  
428 criterion to the size of the satellite instrument's footprint and allow for a time difference as short as possible.  
429 These considerations are to reduce effects of transport, chemistry and boundary layer growth but limit the  
430 number of coinciding observations significantly. We have shown that the spatial distance between the IASI  
431 observations and the FTIR measurement site is of importance: the larger the distance in space, the lower the  
432 correlation. When there is no exact match in the position of both observations the variations in the spatial  
433 separation lead to correlation coefficients that can greatly change even when changing the spatial criteria (xdiff)  
434 from 10 to 30 km. Reasons for the changes are the local nature of NH<sub>3</sub> emissions, the surrounding terrain  
435 characteristics and their influence on local transport of NH<sub>3</sub>. The small values for spatial and temporal  
436 coincidence criteria show the importance of NH<sub>3</sub> sources near the measurement sites when using these  
437 observations for satellite validation. For the validation of the IASI observations, we used a xdiff of less than 25  
438 km, which still showed high correlations while a large number of observations is retained for comparison.

439

440 Overall we see a broad consistency between the IASI and FTIR observations. The seasonal variations of both  
441 datasets look similar for most stations. Increased column values are observed for both IASI and FTIR during  
442 summers as the result of higher temperatures, with some sites showing an increase in concentrations due to  
443 manure application and fertilization events in spring (Bremen, Toronto). In general our comparison shows that  
444 IASI underestimates the NH<sub>3</sub> total columns, except for Wollongong. The Wollongong site has persistent low  
445 background columns, i.e. observations with a low HRI, to which IASI is not very sensitive, which results in an  
446 overestimation of the observed columns. Overall, correlations range from  $r \sim 0.8$  for stations characterised by  
447 higher NH<sub>3</sub> column totals (with FTIR columns up to  $80 \times 10^{15}$  molecules cm<sup>-2</sup>) to low  $r \sim 0.4-0.5$  correlations for  
448 stations, which only have a few to no FTIR observations above  $5 \times 10^{15}$  molecules cm<sup>-2</sup>. Hence, the detection  
449 limit or sensitivity of the IASI instrument largely explain the lower correlation values. The combination of all  
450 sites ( $N_{\text{obs}} = 547$ ) give a MRD of  $-32.4 \pm (56.3) \%$ , a correlation  $r$  of 0.8 with a slope of 0.73.

451

452 In comparison to ground-based in situ systems, the FTIR observations have the big advantage to provide coarse  
453 vertical profiles, from which a column can be derived, which are more similar to what the satellite measures and  
454 therefore more useful for validation. Dedicated NH<sub>3</sub> validation datasets are needed that better match the  
455 overpass times of satellite instruments like IASI, TES and CrIS. This could be achieved by the addition of NH<sub>3</sub>  
456 to the NDACC measurement protocols and matching the overpass time of these satellites over these  
457 measurement stations by using of the right spectral filters for detecting NH<sub>3</sub>. Furthermore, the low number of  
458 NDACC stations and their locations are not optimal for a dedicated validation of NH<sub>3</sub> satellite products.

459 Although these provide a starting point, the small set of stations does not cover the entire range of climate  
460 conditions, agricultural source types and emission regimes. Hence, our validation results should be seen as  
461 indicative. Additional stations or dedicated field campaigns are needed to improve this situation. New stations  
462 should be placed in regions where emissions and geography are homogenous to ensure that stations are  
463 representative for the footprints of the satellites. For validation of satellite products using FTIR measurements a  
464 monitoring and measurements strategy needs to be developed with a representative mixture of locations in  
465 addition to ground level data. The later can cover the spatial variation and different temporal measurements can  
466 be used. The use of IASI and FTIR observations to study NH<sub>3</sub> distributions at ground level requires a  
467 combination of model calculations and observations (e.g. Erisman et al., 2005a; 2005b). Such techniques are  
468 required to provide all the necessary details to describe the high spatial and temporal variations in NH<sub>3</sub>.

469  
470 The direct comparison of the IASI and FTIR columns is an addition to earlier efforts by Van Damme et al.  
471 (2015a) to validate IASI column observations with surface in situ and airborne observations. Our results  
472 presented here indicate that the product performs better than the previously upper bound estimate of a factor 2  
473 (i.e. -50 to +100%) as reported in Van Damme et al. (2014a). Although we tried to diminish any effect of  
474 sampling time and position it cannot be ruled out completely that these impacts the comparison statistics as the  
475 number of stations is small. Still the picture arising from the different stations is rather consistent, which hints at  
476 other issues that may explain the observed bias. A number of important issues concerning the retrieval  
477 techniques may explain the observed difference. First, the HRI based retrieval used for IASI is intrinsically  
478 different to the optimal estimation based approach used for the FTIR retrieval. An IASI optimal estimation  
479 retrieval for NH<sub>3</sub> called FORLI does exist but is not fully operationally used as it is computationally much  
480 slower than the HRI method. Surprisingly a first comparison between the FORLI and HRI based retrieval (see  
481 figure 9, Van Damme et al., 2014a) shows ~30% lower retrieved columns by the HRI scheme, which is very  
482 close to the systematic difference quantified here. Do note that the results are not be fully comparable as the  
483 reported HRI-FORLI comparison was for a limited dataset and no quality selection criteria were applied. We  
484 recommend to further explore the use of the optimal estimation based IASI-NH<sub>3</sub> retrieval in comparison to the  
485 FTIR observations. Second, the IASI and FTIR retrievals incorporate the same line spectroscopy database  
486 (HITRAN 2012; Rothman et al., 2013) which removes a possible error due to different spectroscopy datasets.  
487 The spectroscopy is the largest expected cause of error in the FTIR observations with measurement noise being  
488 the close second for sites with low concentrations. An improvement to the line parameters (i.e. line intensity,  
489 pressure and temperature effects) would greatly benefit both the FTIR and IASI retrievals. Thirdly, the HRI  
490 based scheme uses the difference between spectra with and without the spectral signature of NH<sub>3</sub>. A plausible  
491 cause for error in this scheme is the influence and correlation of interfering species in the same spectral  
492 channels. H<sub>2</sub>O lines occur near most of the NH<sub>3</sub> spectral lines and interfere with the NH<sub>3</sub> lines at the resolution  
493 of the IASI instrument. Humidity levels vary throughout the year with an increase amount of water vapour in  
494 summer conditions. The HRI based scheme uses a fixed amount of water vapour and varying amounts of water  
495 vapour may interfere with the HRI value attributed fully to the NH<sub>3</sub> columns. As there is a seasonality in the  
496 water vapour content of the atmosphere (Wagner et al., 2006), any error attributed to water vapour should show  
497 a seasonality in the difference between the IASI and FTIR observations. A seasonality was, however, not visible  
498 although it may be that the number of coincident observations was too small to recognize it. This again shows

499 the need for dedicated NH<sub>3</sub> validation data (e.a. dedicated FTIR observations). Fourth, the negative bias of the  
500 satellite observations can be expected by the lack of sensitivity to concentrations near the surface. This is of  
501 course where the ammonia concentrations usually peak. The FTIR observations however do fully observe the  
502 lower layers in the troposphere thus causing a discrepancy. Normally one can correct for this using the  
503 averaging kernel of the satellite observations. However, the IASI-NH<sub>3</sub> retrieval does not produce an averaging  
504 kernel meaning it is not possible to calculate the exact effect. The use of a typical averaging kernel will cause  
505 more uncertainty as there is a large day to day variability in the averaging kernels as earlier retrievals showed  
506 (Clarisse et al., 2009). Finally, another possible cause of error is the lack of a varying NH<sub>3</sub> profile and the proxy  
507 used for thermal contrast to describe the state of the atmosphere. The sensitivity of the scheme to the  
508 concentrations of NH<sub>3</sub> in the boundary layer is described by using a fixed profile for land and sea observations  
509 in combination with a thermal contrast based on two layers (surface and 1.5 km) as it is expected that most of  
510 the NH<sub>3</sub> occurs in the boundary layer. In reality the NH<sub>3</sub> profile is highly dynamic due to a varying boundary  
511 layer height and changing emissions as well as temperature changes (e.g. inversions etc) occurring throughout  
512 the planetary boundary layer. Not accounting for this can introduce an error and future HRI based schemes  
513 should focus on estimating the possible effects of using only a specific profile. The use of multiple NH<sub>3</sub>-profiles  
514 in combination with multiple temperature layers would be a better approximation of state of the atmosphere,  
515 although computationally more expensive. The sharp difference between the sea and land retrieval introduces  
516 strong variability in observations near the coast. Furthermore, observations that are directly on the transition  
517 between water and land can introduce problems due to the varying emissivity. Similar issues have been reported  
518 for aerosol retrievals (e.g. Schaap et al., 2008).

519  
520 Although the FTIR observations offer some vertical information, studies combining this technique with tower or  
521 airborne observations are needed to further improve knowledge and sensitivity of the FTIR and satellite  
522 observations to the vertical distribution of NH<sub>3</sub>. Without this knowledge, it is not possible to use the  
523 observations for quantitative emission estimates and modelling purposes as no uncertainty on the new estimate  
524 can be given. Approaches similar to the recent study by Shephard et al. (2015b) using an airborne instrument,  
525 possibly in combination with an FTIR system focused on the overpass of multiple satellite systems for an  
526 extended period of time should be used to establish the sensitivities and biases of the different retrieval products  
527 available from satellite instruments as well as the bias between the satellite and surface instruments. The use of  
528 IASI and FTIR observations to study NH<sub>3</sub> distributions at ground level requires a combination of model  
529 calculations and observations. Such techniques are required to provide all the necessary details to describe the  
530 high spatial and temporal variations in NH<sub>3</sub>.

531

### 532 **Acknowledgements**

533 This work is part of the research programme GO/12-36, which is financed by the Netherlands Organisation for  
534 Scientific Research (NWO). The Lauder NIWA FTIR program is funded through the New Zealand  
535 government's core research grant framework from the Ministry of Business, Innovation and employment. We  
536 thank the Lauder FTIR team for their contribution. Acknowledgements are addressed to the Université de La  
537 Réunion and CNRS (LACy-UMR8105 and UMS3365) for their support of the Reunion Island measurements.  
538 The Reunion Island data analysis has mainly been supported by the A3C project (PRODEX Program of the

539 Belgian Science Policy Office, BELSPO, Brussels). The University of Toronto's NDACC contribution has been  
540 supported by the CAFTON project, funded by the Canadian Space Agency's FAST Program. Measurements  
541 were made at the University of Toronto Atmospheric Observatory (TAO), which has been supported by  
542 CFCAS, ABB Bomem, CFI, CSA, EC, NSERC, ORDCF, PREA, and the University of Toronto. Part of this  
543 research was performed at the Jet Propulsion Laboratory, California Institute of Technology, under contract with  
544 NASA. IASI has been developed and built under the responsibility of the "Centre national d'études spatiales"  
545 (CNES, France). It is flown on-board the Metop satellites as part of the EUMETSAT Polar System. The IASI  
546 L1 data are received through the EUMETCast near real-time data distribution service.  
547 The IASI-related activities in Belgium were funded by Belgian Science Policy Office through the IASI.Flow  
548 Prodex arrangement (2014-2018). PFC, LC and MVD also thank the FRS-FNRS for financial support. L.C. is a  
549 research associate with the Belgian F.R.S-FNRS. C. Clerbaux is grateful to CNES for scientific collaboration  
550 and financial support. The National Center for Atmospheric Research is supported by the National Science  
551 Foundation. The Boulder observation program is supported in part by the Atmospheric Chemistry Observations  
552 & Modeling Division of NCAR. The measurement programme and NDACC site at Wollongong has been  
553 supported by the Australian Research Council for many years, most recent by grant DP110101948 and  
554 LE0668470. The Mexico City site was funded through projects UNAM-DGAPA (109914) and CONACYT  
555 (249374, 239618). A. Bezanilla, J. Baylón and E. Plaza are acknowledged for their participation in the  
556 measurements and analysis. We would like to thank David Griffith, Clare Murphy and Voltaire Velazco at the  
557 School of Chemistry, University of Wollongong, for maintaining FTS instrumentation and conducting FTS  
558 measurements. We are grateful to the many colleagues who have contributed to FTIR data acquisition at the  
559 various sites.

560



561 **References**

- 562  
563 Adams, P.J., Seinfeld, J.H., Koch, D., Mickley, L., Jacob, D. (2001), General circulation model assessment of  
564 direct radiative forcing by the sulfate-nitrate-ammonium-water inorganic aerosol system, *Journal of Geophysical*  
565 *Research Atmospheres*, 106 (1), pp. 1097-1111.
- 566  
567 August, T., Klaes, D., Schlüssel, P., Hultberg, T., Crapeau, M., Arriaga, A., O'Carroll, A., Coppens, D., Munro,  
568 R. and Calbet, X.: IASI on Metop-A: Operational Level 2 retrievals after five years in orbit, *J. Quant. Spectrosc.*  
569 *Radiat. Transf.*, 113(11), 1340–1371, doi:10.1016/j.jqsrt.2012.02.028, 2012.
- 570  
571 Beer, R., Shephard, M. W., Kulawik, S. S., Clough, S. a., Eldering, A., Bowman, K. W., Sander, S. P., Fisher, B.  
572 M., Payne, V. H., Luo, M., Osterman, G. B. and Worden, J. R.: First satellite observations of lower tropospheric  
573 ammonia and methanol, *Geophys. Res. Lett.*, 35(9), 1–5, doi:10.1029/2008GL033642, 2008.
- 574  
575 Bleeker, A., Sutton, M. A., Acherman, B., Alebic-Juretic, A., Aneja, V. P., Ellermann, T., Erisman, J. W., Fowler,  
576 D., Fagerli, H., Gauger, T., Harlen, K. S., Hole, L. R., Horvath, L., Mitosinkova, M., Smith, R. I., Tang, Y. S.,  
577 and Pul, A.: Linking ammonia emission trends to measured concentrations and deposition of reduced nitrogen at  
578 different scales, in: *Atmospheric Ammonia – Detecting emission changes and environmental impacts. Results of*  
579 *an expert workshop under the convention of long-range transboundary air pollution*, edited by: Sutton M. A., Reis  
580 S., Baker S. M. H. , *Atmospheric Ammonia – Detecting emission changes and environmental impacts. Results of*  
581 *an expert workshop under the convention of long-range transboundary air pollution*, Springer, 123–180, 2009.
- 582  
583 Bobbink, R, Hicks K, Galloway J, Spranger T, Alkemade R, Ashmore M, Bustamante M, Cinderby S, Davidson  
584 E, Dentener F, Emmett B, Erisman JW, Fenn M, Gilliam F, Nordin A, Pardo L, De Vries W. Global assessment  
585 of nitrogen deposition effects on terrestrial plant diversity: a synthesis, *Ecological Applications*, 20 (2010), pp.  
586 30–59.
- 587  
588 von Bobruzki, K., Braban, C. F., Famulari, D., Jones, S. K., Blackall, T., Smith, T. E. L., Blom, M., Coe, H.,  
589 Gallagher, M., Ghalaieny, M., McGillen, M. R., Percival, C. J., Whitehead, J. D., Ellis, R., Murphy, J.,  
590 Mohacsi, A., Pogany, A., Junninen, H., Rantanen, S., Sutton, M. A., and Nemitz, E.: Field inter-comparison of  
591 eleven atmospheric ammonia measurement techniques, *Atmos. Meas. Tech.*, 3, 91-112, doi:10.5194/amt-3-91-  
592 2010, 2010.
- 593  
594 Brown, L. R., M. R. Gunson, R. A. Toth, F. W. Irion, C. P. Rinsland, and A. Goldman. "1995 atmospheric trace  
molecule spectroscopy (ATMOS) linelist." *Applied optics* 35, no. 16 (1996): 2828-2848.
- 595  
596 Chang, L., Palo, S., Hagan, M., Richter, J., Garcia, R., Riggin, D. and Fritts, D.: Structure of the migrating diurnal  
597 tide in the Whole Atmosphere Community Climate Model (WACCM), *Advances in Space Research*, 41(9), 1398–  
1407, doi:10.1016/j.asr.2007.03.035, 2008.
- 598  
599 Coheur, P.-F., Clarisse, L., Turquety, S., Hurtmans, D., and Clerbaux, C.: IASI measurements of reactive trace  
species in biomass burning plumes, *Atmos. Chem. Phys.*, 9, 5655-5667, doi:10.5194/acp-9-5655-2009, 2009.
- 600  
601 Clarisse, Lieven, Cathy Clerbaux, Frank Dentener, Daniel Hurtmans, and Pierre-François Coheur. "Global  
ammonia distribution derived from infrared satellite observations." *Nature Geoscience* 2, no. 7 (2009): 479-483.
- 602  
603 Clarisse, L., Shephard, M. W., Dentener, F., Hurtmans, D., Cady-Pereira, K., Karagulian, F., Van Damme, M.,  
604 Clerbaux, C. and Coheur, P.-F.: Satellite monitoring of ammonia: A case study of the San Joaquin Valley, *J.*  
*Geophys. Res.*, 115(D13), 1–15, doi:10.1029/2009JD013291, 2010.
- 605  
606 Dammers, E., Vigouroux, C., Palm, M., Mahieu, E., Warneke, T., Smale, D., Langerock, B., Franco, B., Van  
607 Damme, M., Schaap, M., Notholt, J., and Erisman, J. W.: Retrieval of ammonia from ground-based FTIR solar  
spectra, *Atmos. Chem. Phys.*, 15, 12789-12803, doi:10.5194/acp-15-12789-2015, 2015.
- 608  
609 Dentener, F. J. and Crutzen, P. J.: A three-dimensional model of the global ammonia cycle, *J. Atmos. Chem.*,  
19(4), 331–369, doi:10.1007/BF00694492, 1994.
- 610  
611 Dentener, F., Drevet, J., Lamarque, J. F., Bey, I., Eickhout, B., Fiore, A. M., Hauglustaine, D., Horowitz, L. W.,  
612 Krol, M., Kulshrestha, U. C., Lawrence, M., Galy-Lacaux, C., Rast, S., Shindell, D., Stevenson, D., Van Noije,  
613 T., Atherton, C., Bell, N., Bergman, D., Butler, T., Cofala, J., Collins, B., Doherty, R., Ellingsen, K., Galloway,  
J., Gauss, M., Montanaro, V., Müller, J. F., Pitari, G., Rodriguez, J., Sanderson, M., Solmon, F., Strahan, S.,

614 Schultz, M., Sudo, K., Szopa, S. and Wild, O.: Nitrogen and sulfur deposition on regional and global scales: A  
615 multimodel evaluation, *Global Biogeochem. Cycles*, 20(4), doi:10.1029/2005GB002672, 2006.  
616  
617  
618 Dils, B., De Mazière, M., Müller, J. F., Blumenstock, T., Buchwitz, M., de Beek, R., Demoulin, P., Duchatelet, P.,  
619 Fast, H., Frankenberg, C., Gloudemans, A., Griffith, D., Jones, N., Kerzenmacher, T., Kramer, I., Mahieu, E.,  
620 Mellqvist, J., Mittermeier, R. L., Notholt, J., Rinsland, C. P., Schrijver, H., Smale, D., Strandberg, A.,  
621 Straume, A. G., Stremme, W., Strong, K., Sussmann, R., Taylor, J., van den Broek, M., Velazco, V., Wagner, T.,  
622 Warneke, T., Wiacek, A., and Wood, S.: Comparisons between SCIAMACHY and ground-based FTIR data for  
623 total columns of CO, CH<sub>4</sub>, CO<sub>2</sub> and N<sub>2</sub>O, *Atmos. Chem. Phys.*, 6, 1953-1976, doi:10.5194/acp-6-1953-2006,  
624 2006.

625 EDGAR-Emission Database for Global Atmospheric Research: Source: EC-JRC/PBL. EDGAR version 4.2.,  
626 <http://edgar.jrc.ec.europa.eu>, access 15th October 2012, 2011  
627

628 Erisman, J. W., Hensen, A., Mosquera, J., Sutton, M. and Fowler, D.: Deposition monitoring networks: what  
629 monitoring is required to give reasonable estimates of ammonia/ammonium?, *Environ. Pollut.*, 135(3), 419–431,  
630 doi:<http://dx.doi.org/10.1016/j.envpol.2004.11.015>, 2005a.  
631

632 Erisman, J. W., Vermeulen, A., Hensen, A., Flechard, C., Dämmgen, U., Fowler, D., Sutton, M., Grünhage, L.  
633 and Tuovinen, J. P.: Monitoring and modelling of biosphere/atmosphere exchange of gases and aerosols in  
634 Europe, *Environ. Pollut.*, 133(3), 403–413, doi:10.1016/j.envpol.2004.07.004, 2005b.  
635

636 Erisman, J. W., Bleeker, a., Galloway, J. and Sutton, M. S.: Reduced nitrogen in ecology and the environment,  
637 *Environ. Pollut.*, 150(1), 140–149, doi:10.1016/j.envpol.2007.06.033, 2007.  
638

639 Erisman, J. W., Sutton, M. a., Galloway, J., Klimont, Z. and Winiwarter, W.: How a century of ammonia synthesis  
640 changed the world, , 1(October 1908), doi:10.1038/ngeo325, 2008.  
641

642 Erisman, J. W., Galloway, J., Seitzinger, S., Bleeker, A. and Butterbach-Bahl, K.: Reactive nitrogen in the  
643 environment and its effect on climate change, *Curr. Opin. Environ. Sustain.*, 3(5), 281–290,  
644 doi:10.1016/j.cosust.2011.08.012, 2011.  
645

646 Farr, T. G., Rosen, P. a., Caro, E. and Crippen, R.: The Shuttle Radar Topography Mission, *Rev. ...*, (2005), 1–  
647 33, doi:10.1029/2005RG000183.1.INTRODUCTION, 2007.  
648

649 Fowler, D., Coyle, M., Skiba, U., Sutton, M. A., Cape, J. N., Reis, S., Sheppard, L. J., Jenkins, A., Grizzetti, B.,  
650 Galloway, J. N., Vitousek, P., Leach, A., Bouwman, A. F., Butterbach-Bahl, K., Dentener, F., Stevenson, D.,  
651 Amann, M. and Voss, M.: The global nitrogen cycle in the twenty-first century, *Philos. Trans. R. Soc. London B*  
652 *Biol. Sci.*, 368(1621) [online] Available from:  
653 <http://rstb.royalsocietypublishing.org/content/368/1621/20130164.abstract>, 2013.  
654

655 Griesfeller, a., Griesfeller, J., Hase, F., Kramer, I., Loës, P., Mikuteit, S., Raffalski, U., Blumenstock, T. and  
656 Nakajima, H.: Comparison of ILAS-II and ground-based FTIR measurements of O<sub>3</sub>, HNO<sub>3</sub>, N<sub>2</sub>O, and CH<sub>4</sub>  
657 over Kiruna, Sweden, *J. Geophys. Res.*, 111(D11), D11S07, doi:10.1029/2005JD006451, 2006.  
658

659 Hase, F., Blumenstock, T. and Paton-Walsh, C.: Analysis of the instrumental line shape of high-resolution  
660 fourier transform IR spectrometers with gas cell measurements and new retrieval software., *Appl. Opt.*, 38(15),  
661 3417–3422, 1999.  
662

663 Hase, F., Hannigan, J. W., Coffey, M. T., Goldman, a., Höpfner, M., Jones, N. B., Rinsland, C. P. and Wood, S.  
664 W.: Intercomparison of retrieval codes used for the analysis of high-resolution, ground-based FTIR  
665 measurements, *J. Quant. Spectrosc. Radiat. Transf.*, 87(1), 25–52, doi:10.1016/j.jqsrt.2003.12.008, 2004.  
666

667 Hase, F., Demoulin, P., Sauval, A. J., Toon, G. C., Bernath, P. F., Goldman, A., Hannigan, J. W., Rinsland, C. P.:  
668 An empirical line-by-line model for the infrared solar transmittance spectrum from 700 to 5000 cm<sup>-1</sup>, *J. Quant.*  
669 *Spectrosc. Ra.*, 102, 450–463, doi:10.1016/j.jqsrt.2006.02.026, 2006.  
670

671 Holland, E. a., Dentener, F. J., Braswell, B. H. and Sulzman, J. M.: Contemporary and pre-industrial global  
672 reactive nitrogen budgets, *Biogeochemistry*, 46(1-3), 7–43, doi:10.1007/BF01007572, 1999.

673  
674 Irie, H., Boersma, K. F., Kanaya, Y., Takashima, H., Pan, X. and Wang, Z. F.: Quantitative bias estimates for  
675 tropospheric NO<sub>2</sub> columns retrieved from SCIAMACHY, OMI, and GOME-2 using a common standard for  
676 East Asia, *Atmos. Meas. Tech.*, 5(10), 2403–2411, doi:10.5194/amt-5-2403-2012, 2012.  
677  
678 Kerzenmacher, T., Dils, B., Kumps, N., Blumenstock, T., Clerbaux, C., Coheur, P.-F., Demoulin, P., García, O.,  
679 George, M., Griffith, D. W. T., Hase, F., Hadji-Lazaro, J., Hurtmans, D., Jones, N., Mahieu, E., Notholt, J., Paton-  
680 Walsh, C., Raffalski, U., Ridder, T., Schneider, M., Servais, C., and De Mazière, M.: Validation of IASI FORLI  
681 carbon monoxide retrievals using FTIR data from NDACC, *Atmos. Meas. Tech.*, 5, 2751–2761, doi:10.5194/amt-  
682 5-2751-2012, 2012.  
683  
684  
685 Leen, J. B., Yu, X. Y., Gupta, M., Baer, D. S., Hubbe, J. M., Kluzek, C. D., Tomlinson, J. M. and Hubbell, M. R.:  
686 Fast in situ airborne measurement of ammonia using a mid-infrared off-axis ICOS spectrometer, *Environ. Sci.*  
687 *Technol.*, 47(18), 10446–10453, doi:10.1021/es401134u, 2013.  
688  
689 Luo, M., Shephard, M. W., Cady-Pereira, K. E., Henze, D. K., Zhu, L., Bash, J. O., Pinder, R. W., Capps, S. L.,  
690 Walker, J. T. and Jones, M. R.: Satellite observations of tropospheric ammonia and carbon monoxide: Global  
691 distributions, regional correlations and comparisons to model simulations, *Atmos. Environ.*, 106, 262–277,  
692 doi:10.1016/j.atmosenv.2015.02.007, 2015.  
693  
694 Lutsch, E., Dammers, E., Conway, S. and Strong, K: Ground-based FTIR measurements of CO, HCN, C<sub>2</sub>H<sub>6</sub> and  
695 NH<sub>3</sub> emissions from the 2014 Canadian Wildfires, *in preparation*.  
696  
697 Morgenstern, O., Zeng, G., Wood, S. W., Robinson, J., Smale, D., Paton-Walsh, C., Jones, N. B., and Griffith,  
698 D. W. T.: Long-range correlations in Fourier transform infrared, satellite, and modeled CO in the Southern  
699 Hemisphere, *J. Geophys. Res.*, 117, D11301 doi:10.1029/2012JD017639, 2012.  
700  
701 Moya, M., Fountoukis, C., Nenes, A., Matías, E., and Grutter, M.: Predicting diurnal variability of fine  
702 inorganic aerosols and their gas-phase precursors near downtown Mexico City, *Atmos. Chem. Phys. Discuss.*, 7,  
703 11257–11294, doi:10.5194/acpd-7-11257-2007, 2007.  
704  
705 Nowak, J. B., Neuman, J. A., Kozai, K., Huey, L. G., Tanner, D. J., Holloway, J. S., Ryerson, T. B., Frost, G. J.,  
706 McKeen, S. A., and Fehsenfeld, F. C.: A chemical ionization mass spectrometry technique for airborne  
707 measurements of ammonia, *J. Geophys. Res.-Atmos.*, 112, D10S02, doi:10.1029/2006JD007589, 2007.  
708  
709 Nowak, J. B., Neuman, J. A., Bahreini, R., Brock, C. A., Middlebrook, A. M., Wollny, A. G., Holloway, J. S.,  
710 Peischl, J., Ryerson, T. B., and Fehsenfeld, F. C.: Airborne observations of ammonia and ammonium nitrate  
711 formation over Houston, Texas, *J. Geophys. Res.-Atmos.*, 115, D22 304, doi:10.1029/ 2010JD014195, 2010.  
712  
713 Ohyama, H., Morino, I., Nagahama, T., Machida, T., Suto, H., Oguma, H., Sawa, Y., Matsueda, H., Sugimoto,  
714 N., Nakane, H., and Nakagawa, K.: Column-averaged volume mixing ratio of CO<sub>2</sub> measured with ground-based  
715 Fourier transform spectrometer at Tsukuba, *J. Geophys. Res.*, 114, D18303, doi:10.1029/2008JD011465, 2009.  
716  
717 Paton-Walsh, C., Jones, N. B., Wilson, S. R., Haverd, V., Meier, A., Griffith, D. W. T. and Rinsland, C. P.  
718 (2005), Measurements of trace gas emissions from Australian forest fires and correlations with coincident  
719 measurements of aerosol optical depth, *J. Geophys. Res.*, 110, D24305, doi:10.1029/2005JD006202  
720  
721 Pope, III, C. A., Ezzati, M., and Dockery, D. W.: Fine-Particulate Air Pollution and Life Expectancy in the United  
722 States, *N. Engl. J. Med.*, 360, 376–386, doi:10.1056/NEJMsa0805646, 2009.  
723  
724 Pougatchev, N. S., Connor, B. J., & Rinsland, C. P. (1995). Infrared measurements of the ozone vertical  
725 distribution above Kitt Peak. *Journal of Geophysical Research: Atmospheres (1984–2012)*, 100(D8), 16689-  
726 16697.  
727  
728 Puchalski, M. A., M. E. Sather, J. T. Walker, C. M. Lehmann, D. A. Gay, J. Mathew, and W. P. Robarge (2011),  
729 Passive ammonia monitoring in the United States: Comparing three different sampling devices, *J. Environ. Monit.*,  
730 13(11), 3156–3167, doi:10.1039/c1em10553a.  
731

732 Ravishankara, A. R., Daniel, J. S. and Portmann, R. W.: Nitrous oxide (N<sub>2</sub>O): the dominant ozone-depleting  
733 substance emitted in the 21st century., *Science*, 326(5949), 123–125, doi:10.1126/science.1176985, 2009.  
734

735 Rockstrom, J., Steffen, W., Noone, K., Persson, A., Chapin, F. S., Lambin, E. F., Lenton, T. M., Scheffer, M.,  
736 Folke, C., Schellnhuber, H. J., Nykvist, B., de Wit, C. A., Hughes, T., van der Leeuw, S., Rodhe, H., Sorlin, S.,  
737 Snyder, P. K., Costanza, R., Svedin, U., Falkenmark, M., Karlberg, L., Corell, R. W., Fabry, V. J., Hansen, J.,  
738 Walker, B., Liverman, D., Richardson, K., Crutzen, P. and Foley, J. A.: A safe operating space for humanity,  
739 *Nature*, 461(7263), 472–475 [online] Available from: <http://dx.doi.org/10.1038/461472a>, 2009.  
740

741 Rodgers, C. D.: *Inverse Methods for Atmospheric Sounding - Theory and Practice*, 2(January), 256,  
742 doi:10.1142/9789812813718, 2000.  
743

744 Rodgers, C. D. and Connor, B. J.: Intercomparison of remote sounding instruments, *J. Geophys. Res. Atmos.*,  
745 108(D3), n/a–n/a, doi:10.1029/2002JD002299, 2003.  
746

747 Rodhe, Henning, Frank Dentener, and Michael Schulz. "The global distribution of acidifying wet  
748 deposition." *Environmental Science & Technology* 36.20 (2002): 4382-4388.  
749

750 Rothman, L. S., Gordon, I. E., Babikov, Y., Barbe, a., Chris Benner, D., Bernath, P. F., Birk, M., Bizzocchi, L.,  
751 Boudon, V., Brown, L. R., Campargue, a., Chance, K., Cohen, E. a., Coudert, L. H., Devi, V. M., Drouin, B. J.,  
752 Fayt, a., Flaud, J. M., Gamache, R. R., Harrison, J. J., Hartmann, J. M., Hill, C., Hodges, J. T., Jacquemart, D.,  
753 Jolly, a., Lamouroux, J., Le Roy, R. J., Li, G., Long, D. a., Lyulin, O. M., Mackie, C. J., Massie, S. T.,  
754 Mikhailenko, S., Müller, H. S. P., Naumenko, O. V., Nikitin, a. V., Orphal, J., Perevalov, V., Perrin, a.,  
755 Polovtseva, E. R., Richard, C., Smith, M. a H., Starikova, E., Sung, K., Tashkun, S., Tennyson, J., Toon, G. C.,  
756 Tyuterev, V. G. and Wagner, G.: The HITRAN2012 molecular spectroscopic database, *J. Quant. Spectrosc.*  
757 *Radiat. Transf.*, 130, 4–50, doi:10.1016/j.jqsrt.2013.07.002, 2013.  
758

759 Schaap, M., van Loon, M., ten Brink, H. M., Dentener, F. J., and Bultjes, P. J. H.: Secondary inorganic aerosol  
760 simulations for Europe with special attention to nitrate, *Atmos. Chem. Phys.*, 4, 857-874, doi:10.5194/acp-4-857-  
761 2004, 2004  
762

763 Schaap, M., Timmermans, R. M. a, Koelemeijer, R. B. a, de Leeuw, G. and Bultjes, P. J. H.: Evaluation of  
764 MODIS aerosol optical thickness over Europe using sun photometer observations, *Atmos. Environ.*, 42(9), 2187–  
765 2197, doi:10.1016/j.atmosenv.2007.11.044, 2008.  
766

767 Senten, C., De Mazière, M., Dils, B., Hermans, C., Kruglanski, M., Neefs, E., Scolas, F., Vandaele, A. C.,  
768 Vanhaelewyn, G., Vigouroux, C., Carleer, M., Coheur, P. F., Fally, S., Barret, B., Baray, J. L., Delmas, R., Leveau,  
769 J., Metzger, J. M., Mahieu, E., Boone, C., Walker, K. A., Bernath, P. F., and Strong, K.: Technical Note: New  
770 ground-based FTIR measurements at Ile de La Réunion: observations, error analysis, and comparisons with  
771 independent data, *Atmos. Chem. Phys.*, 8, 3483-3508, doi:10.5194/acp-8-3483-2008, 2008.  
772

773 Shephard, M. W., Cady-Pereira, K. E., Luo, M., Henze, D. K., Pinder, R. W., Walker, J. T., Rinsland, C. P.,  
774 Bash, J. O., Zhu, L., Payne, V. H., and Clarisse, L.: TES ammonia retrieval strategy and global observations of  
775 the spatial and seasonal variability of ammonia, *Atmos. Chem. Phys.*, 11, 10743-10763, doi:10.5194/acp-11-  
776 10743-2011, 2011.

777 Shephard, M. W. and Cady-Pereira, K. E.: Cross-track Infrared Sounder (CrIS) satellite observations of  
778 tropospheric ammonia, *Atmos. Meas. Tech.*, 8, 1323-1336, doi:10.5194/amt-8-1323-2015, 2015a.

779 Shephard, M. W., McLinden, C. A., Cady-Pereira, K. E., Luo, M., Moussa, S. G., Leithead, A., Liggio, J., Staebler,  
780 R. M., Akingunola, A., Makar, P., Lehr, P., Zhang, J., Henze, D. K., Millet, D. B., Bash, J. O., Zhu, L., Wells, K.  
781 C., Capps, S. L., Chaliyakunnel, S., Gordon, M., Hayden, K., Brook, J. R., Wolde, M., and Li, S.-M.: Tropospheric  
782 Emission Spectrometer (TES) satellite validations of ammonia, methanol, formic acid, and carbon monoxide over  
783 the Canadian oil sands, *Atmos. Meas. Tech. Discuss.*, 8, 9503-9563, doi:10.5194/amtd-8-9503-2015, 2015b.

784 Slanina, J., ten Brink, H. M., Otjes, R. P., Even, A., Jongejan, P., Khlystov, A., Waijers-Ijpelaar, A., Hu, M., and  
785 Lu, Y.: Continuous analysis of nitrate and ammonium in aerosols by the Steam Jet Aerosol Collector (SJAC),  
786 *Atmos. Environ.*, 35, 2319–2330, 2001.

877 Stremme, W., Ortega, I., and Grutter, M.: Using ground-based solar and lunar infrared spectroscopy to study the  
878 diurnal trend of carbon monoxide in the Mexico City boundary layer, *Atmos. Chem. Phys.*, 9, 8061-8078,  
879 doi:10.5194/acp-9-8061-2009, 2009.

790 Stremme, W., Grutter, M., Rivera, C., Bezanilla, A., Garcia, A. R., Ortega, I., George, M., Clerbaux, C., Coheur,  
791 P.-F., Hurtmans, D., Hannigan, J. W., and Coffey, M. T.: Top-down estimation of carbon monoxide emissions  
792 from the Mexico Megacity based on FTIR measurements from ground and space, *Atmos. Chem. Phys.*, 13, 1357-  
793 1376, doi:10.5194/acp-13-1357-2013, 2013.

794 Sutton, M., Stefan Reis, and Samantha MH Baker. "Atmospheric ammonia." *Detecting Emission Changes and*  
795 *Environmental Impacts* 494 (2009).

796 Sutton, M. a, Reis, S., Riddick, S. N., Dragosits, U., Nemitz, E., Theobald, M. R., Tang, Y. S., Braban, C. F.,  
797 Vieno, M., Dore, A. J., Mitchell, R. F., Wanless, S., Daunt, F., Fowler, D., Blackall, T. D., Milford, C., Flechard,  
798 C. R., Loubet, B., Massad, R., Cellier, P., Personne, E., Coheur, P. F., Clarisse, L., Van Damme, M., Ngadi, Y.,  
799 Clerbaux, C., Skj  th, C. A., Geels, C., Hertel, O., Wichink Kruit, R. J., Pinder, R. W., Bash, J. O., Walker, J. T.,  
800 Simpson, D., Horv  th, L., Misselbrook, T. H., Bleeker, A., Dentener, F. and de Vries, W.: Towards a climate-  
801 dependent paradigm of ammonia emission and deposition., *Philos. Trans. R. Soc. Lond. B. Biol. Sci.*, 368(1621),  
802 20130166, doi:10.1098/rstb.2013.0166, 2013.

803 Sun, K., Cady-Pereira, K., Miller, D. J. , Tao, L., Zondlo, M.A. , Nowak, J. B., Neuman, J. A., Mikoviny, T.,  
804 M  ller, M. , Wisthaler, A., Scarino, A. J., and Hostetler, C. A.: Validation of TES ammonia observations at the  
805 single pixel scale in the San Joaquin Valley during DISCOVER-AQ, *J. Geophys. Res.-Atmos.*, 120, 5140–5154,  
806 doi:10.1002/2014JD022846, 2015.

807  
808 Toon, G. C., Blavier, J.-F., Sen, B., Margitan, J. J., Webster, C. R., Max, R. D., Fahey, D. W., Gao, R., DelNegro,  
809 L., Proffitt, M., Elkins, J., Romashkin, P. A., Hurst, D. F., Oltmans, S., Atlas, E., Schauffler, S., Flocke, F., Bui,  
810 T. P., Stimpfle, R. M., Bonne, G. P., Voss, P. B., and Cohen, R. C.: Comparison of MkIV balloon and ER-2  
811 aircraft measurements of atmospheric trace gases, *J. Geophys. Res.*, 104, 26 779–26 790, 1999.

812  
813 Van Damme, M., Clarisse, L., Heald, C. L., Hurtmans, D., Ngadi, Y., Clerbaux, C., Dolman, A. J., Erisman, J. W.,  
814 and Coheur, P. F.: Global distributions, time series and error characterization of atmospheric ammonia (NH<sub>3</sub>) from  
815 IASI satellite observations, *Atmos. Chem. Phys.*, 14, 2905-2922, doi:10.5194/acp-14-2905-2014, 2014a.

816  
817 Van Damme, M., R. J. Wichink Kruit, M. Schaap, L. Clarisse, C. Clerbaux, P.-F. Coheur, E. Dammers, A. J.  
818 Dolman, and J. W. Erisman , Evaluating 4 years of atmospheric ammonia (NH<sub>3</sub>) over Europe using IASI satellite  
819 observations and LOTOS-EUROS model results, *J. Geophys. Res. Atmos.*, 119, 9549–9566,  
820 doi:[10.1002/2014JD021911](https://doi.org/10.1002/2014JD021911), 2014b.

821  
822 Van Damme, M., Clarisse, L., Dammers, E., Liu, X., Nowak, J. B., Clerbaux, C., Flechard, C. R., Galy-Lacaux,  
823 C., Xu, W., Neuman, J. a., Tang, Y. S., Sutton, M. a., Erisman, J. W. and Coheur, P. F.: Towards validation of  
824 ammonia (NH<sub>3</sub>) measurements from the IASI satellite, *Atmos. Meas. Tech.*, 8(3), 1575–1591, doi:10.5194/amt-  
825 8-1575-2015, 2015a.

826  
827 Van Damme, M., J. W. Erisman, L. Clarisse, E. Dammers, S. Whitburn, C. Clerbaux, A. J. Dolman, and P.-F.  
828 Coheur (2015b), Worldwide spatiotemporal atmospheric ammonia (NH<sub>3</sub>) columns variability revealed by  
829 satellite, *Geophys. Res. Lett.*, 42, doi:10.1002/2015GL065496.

830  
831 Velazco, V., Wood, S. W., Sinnhuber, M., Kramer, I., Jones, N. B., Kasai, Y., Notholt, J., Warneke, T.,  
832 Blumenstock, T., Hase, F., Murcray, F. J., and Schrems, O.: Annual variation of strato-mesospheric carbon  
833 monoxide measured by ground-based Fourier transform infrared spectrometry, *Atmos. Chem. Phys.*, 7, 1305-  
834 1312, doi:10.5194/acp-7-1305-2007, 2007.

835  
836 Vigouroux, C., Hendrick, F., Stavroukou, T., Dils, B., De Smedt, I., Hermans, C., Merlaud, A., Scolas, F., Senten,  
837 C., Vanhaelewyn, G., Fally, S., Carleer, M., Metzger, J.-M., M  ller, J.-F., Van Roozendaal, M., and De  
838 Mazi  re, M.: Ground-based FTIR and MAX-DOAS observations of formaldehyde at R  union Island and  
839 comparisons with satellite and model data, *Atmos. Chem. Phys.*, 9, 9523-9544, doi:10.5194/acp-9-9523-2009,  
840 2009.

841

842 Wagner, T., Beirle, S., Grzegorski, M. and Platt, U.: Global trends (1996-2003) of total column precipitable  
843 water observed by Global Ozone Monitoring Experiment (GOME) on ERS-2 and their relation to near-surface  
844 temperature, *J. Geophys. Res. Atmos.*, 111(12), 1–15, doi:10.1029/2005JD006523, 2006.  
845

846 Whitburn, S., Van Damme, M., Kaiser, J. W., van der Werf, G. R., Turquety, S., Hurtmans, D., Clarisse, L.,  
847 Clerbaux, C. and Coheur, P.-F.: Ammonia emissions in tropical biomass burning regions: Comparison between  
848 satellite-derived emissions and bottom-up fire inventories, *Atmos. Environ.*, 1–13,  
849 doi:10.1016/j.atmosenv.2015.03.015, 2015.  
850

851 Whitburn, S. Van Damme, M., Clarisse, L., Heald, C., Bauduin, S., Hadji-Lazaro, J., Hurtmans, D., Clerbaux,  
852 C. and Coheur P.-F.: A flexible and robust IASI-NH 3 retrieval algorithm, 2015 (in preparation)  
853

854 Wiacek, A., Taylor, J. R., Strong, K., Saari, R., Kerzenmacher, T. E., Jones, N. B. and Griffith, D. W. T.:  
855 Ground-Based Solar Absorption FTIR Spectroscopy: Characterization of Retrievals and First Results from a  
856 Novel Optical Design Instrument at a New NDACC Complementary Station, *J. Atmos. Ocean. Technol.*, 24(3),  
857 432–448, doi:10.1175/JTECH1962.1, 2007.  
858

859 Wood, S. W.: Validation of version 5.20 ILAS HNO<sub>3</sub>, CH<sub>4</sub>, N<sub>2</sub>O, O<sub>3</sub>, and NO<sub>2</sub> using ground-based  
860 measurements at Arrival Heights and Kiruna, *J. Geophys. Res.*, 107(D24), 8208, doi:10.1029/2001JD000581,  
861 2002.  
862

863 Zhu, L., Henze, D. K., Cady-Pereira, K. E., Shephard, M. W., Luo, M., Pinder, R. W., Bash, J. O. and Jeong, G.  
864 R.: Constraining U.S. ammonia emissions using TES remote sensing observations and the GEOS-Chem adjoint  
865 model, *J. Geophys. Res. Atmos.*, 118(8), 3355–3368, doi:10.1002/jgrd.50166, 2013.  
866

## Tables

**Table 1** FTIR stations used in the analysis. The location, longitude, latitude and altitude are given for each station as well as the instrument used for the measurements. Typical emission sources are mentioned in the station specifics tab. The topography describes the geography of the region surrounding the site. N gives the number of observations made during the period of interest. Time period gives the period from which data is used. The last columns describes the used algorithm for the retrieval.

Station Location	Lon	Lat	Altitude (m.a.s.l.)	Instrument	Station specifics	Topography	Time period	N	Retrieval type
Bremen, Germany	8.85E	53.10N	27	Bruker 125 HR	City, fertilizers, livestock	Flat	2008-2015	278	Normal
Toronto, Canada	79.60W	43.66N	174	ABB Bomem DA8	City, fertilizers, biomass burning	On the edge of lake Ontario	2008-2015	1167	Normal
Boulder, United States	105.26W	39.99N	1634	Bruker 120 HR	Fertilizers, biomass burning, livestock	Mountain range to the west	2010-2015	440	Normal
Tsukuba, Japan	140.13E	36.05N	31	Bruker 125 HR	Fertilizers, city	Mostly flat, hills to the north	2014-2015	66	Normal
Pasadena, United States	118.17W	34.20N	460	MKIV_JPL	City, fertilizers, biomass burning	Mountain range to the east	2010-2015	695	Normal
Mexico City, Mexico	99.18W	19.33N	2260	Bruker Vertex 80	City, fires, fertilizers	In between mountain ranges	2012-2015	3980	Normal
St.-Denis, Reunion	55.5E	20.90S	85	Bruker 120 M	Fertilizers, biomass burning, remote	Volcanic	2008-2012	948	Wide
Wollongong, Australia	150.88E	34.41S	30	Bruker 125 HR	Fertilizers, biomass burning, low emissions	Coastal, hills to the west	2008-2015	3641	Wide
Lauder, New Zealand	169.68E	45.04S	370	Bruker 120 HR	Fertilizers, livestock	Hills	2008-2015	1784	Normal

**Table 2** Applied data filters to the IASI-NH<sub>3</sub> product.

Filter	Filter Criteria
Elevation	$ \text{FTIRstation} - \text{IASI\_Observation}  < 300 \text{ m}$
Thermal Contrast	Thermal contrast $> 12 \text{ K}$
Surface Temperature	$T > 275.15 \text{ K}$
IASI-NH <sub>3</sub> retrieval Error	None
Cloud cover fraction	$< 10\%$
Spatial sampling difference	$50 \text{ km} \rightarrow 10 \text{ km}, \Delta x = 5 \text{ km}$
Temporal sampling difference	$< 90 \text{ minutes}$

Table 3. Summarized results of the comparison between FTIR-NH<sub>3</sub> and IASI-NH<sub>3</sub> total columns within the coincidence criteria threshold (xdiff < 25 km, tdiff < 90minutes). N is the number of averaged total columns, **MRD** is the Mean Relative Difference (in %), **r** and **slope** are the correlation coefficient and slope of the linear regression.

Sites	N	MRD in % (rms 1 $\sigma$ )	r	slope
Bremen	53	-22.5 $\pm$ (54.0)	0.83	0.60
Toronto	170	-46.0 $\pm$ (47.0)	0.79	0.84
Boulder	38	-38.2 $\pm$ (43.5)	0.76	1.11
Tsukuba	15	-28.3 $\pm$ (35.6)	0.67	0.57
Pasadena	16	-47.9 $\pm$ (30.1)	0.59	0.83
Mexico	65	-30.8 $\pm$ (43.9)	0.64	1.14
St.-Denis	20	-61.3 $\pm$ (78.7)	0.65	1.26
Wollongong	62	6.0 $\pm$ (74.3)	0.47	0.92
Lauder	108	-29.7 $\pm$ (57.3)	0.55	0.77
<b>Combined</b>	<b>547</b>	<b>-32.4<math>\pm</math>(56.3)</b>	<b>0.80</b>	<b>0.73</b>



## Figures

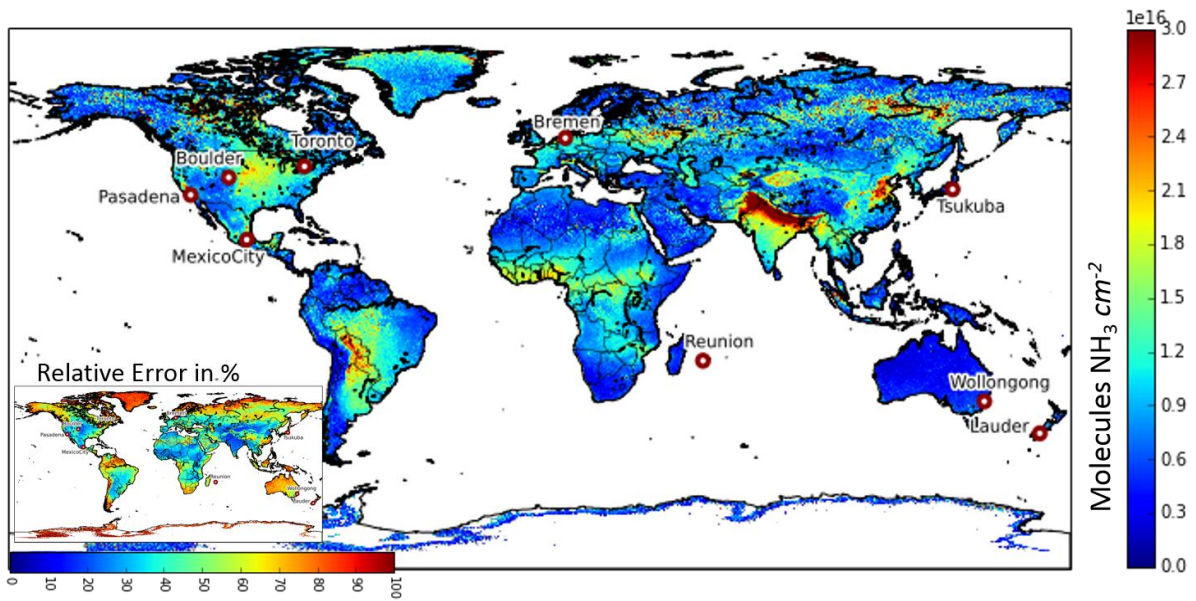


Figure 1. Mean IASI-NH<sub>3</sub> total column distribution for the period between January 2008 and January 2015. The total columns are a weighted average of the individual observations weighted with the relative error. Red circles indicate the positions of the FTIR stations.

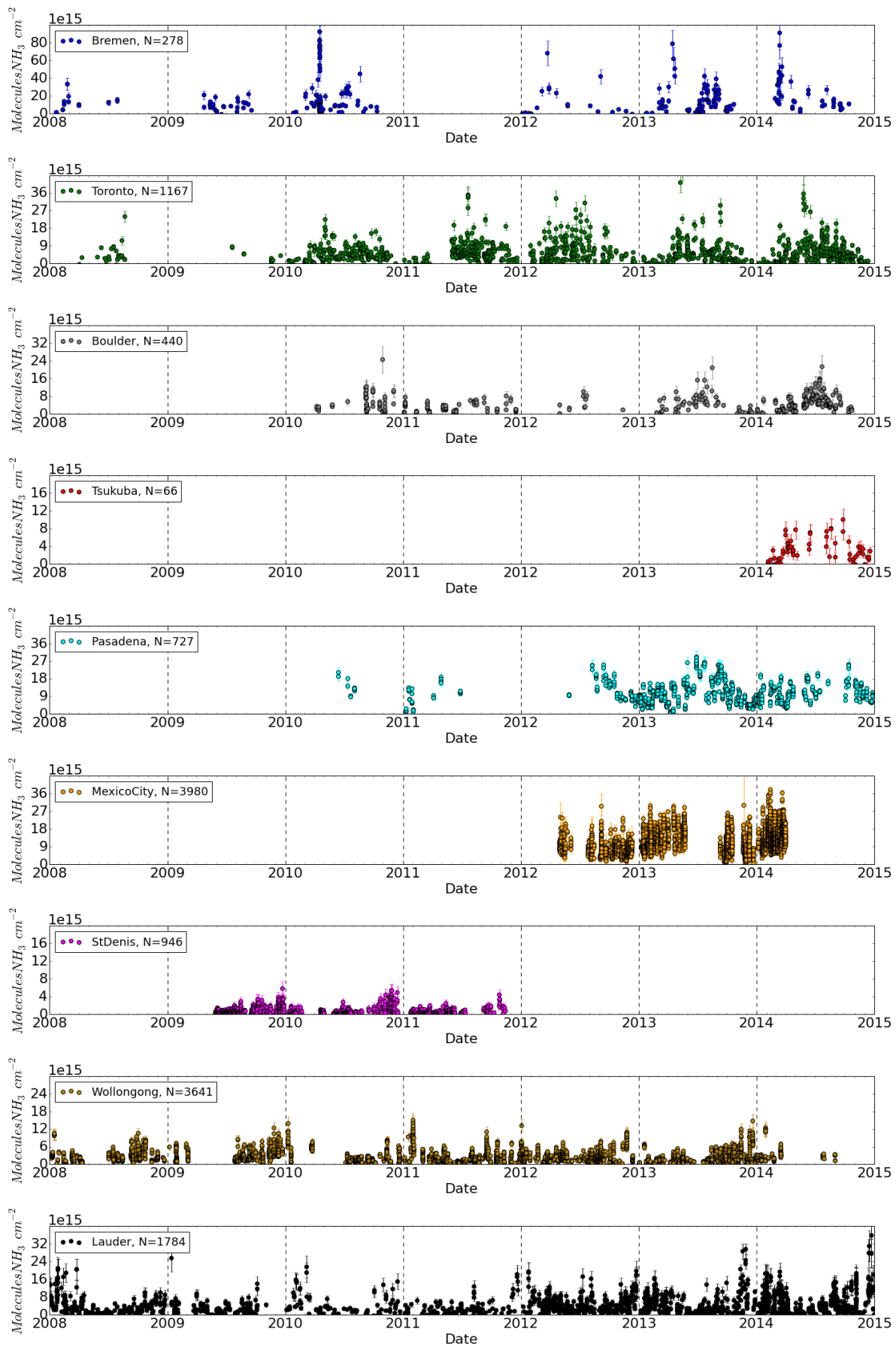


Figure 2. FTIR retrieved NH<sub>3</sub> Total Columns (in *molecules cm<sup>-2</sup>*). Note, the labels on the vertical axis vary for each site.

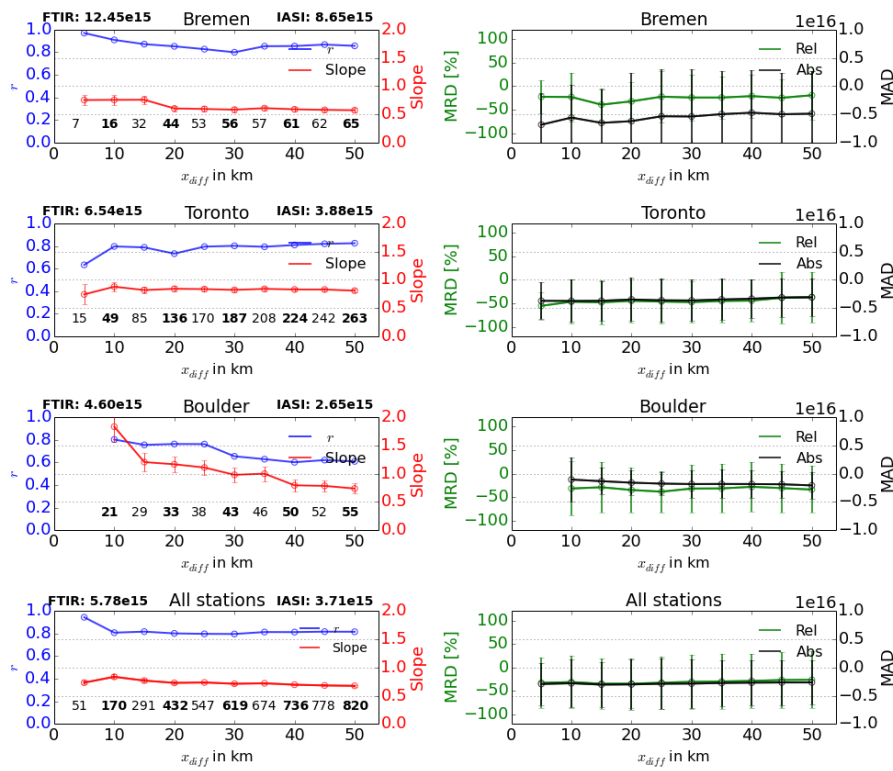


Figure 3. Correlation  $r$  (Blue lines, left figures), slope (Red lines, left figures) regression results, Mean Relative Difference (MRD, green lines, right figures) and Mean Absolute Difference (MAD, black lines, right figures) between IASI and FTIR observations as a function of  $x_{diff}$  for a selection of sites. Bars indicate the standard deviation of the slope of the individual regression results. The numbers in the bottom of each subfigure show the number of matching observations. The numbers on the left and right side of the stations name give the mean FTIR and IASI total columns for a  $x_{diff} < 25$  km.

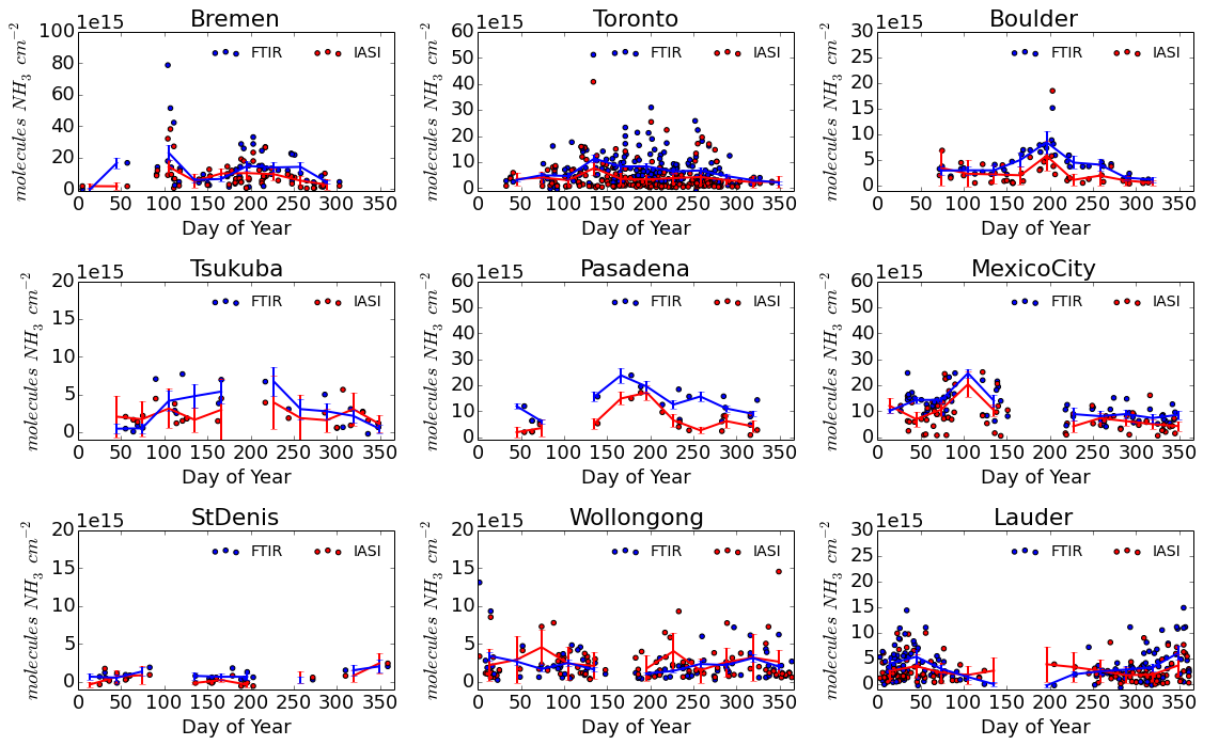


Figure 4. Time series of  $\text{NH}_3$  for IASI and FTIR datasets with  $\text{xdiff} < 25$  km and  $\text{tdiff} < 90$  minutes (FTIR: Blue and IASI: Red). Scattered values are the observations for each day of year (multiple years of observations). The lines show the monthly mean total columns of the respective sets.

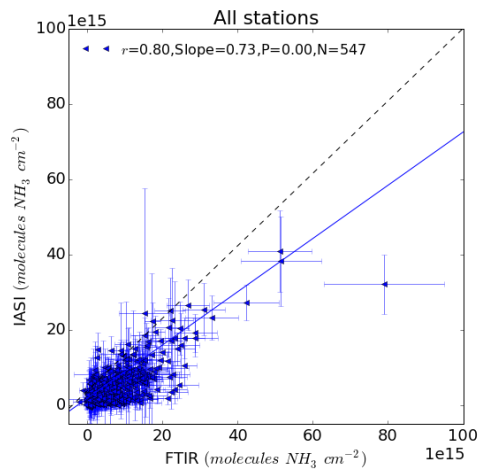


Figure 5. Correlations between the FTIR and IASI total columns with filters thermal contrast  $> 12\text{K}$ ,  $\text{tdiff} < 90$  min,  $\text{xdiff} < 25$  km. The trend line shows the results of the regression analysis.

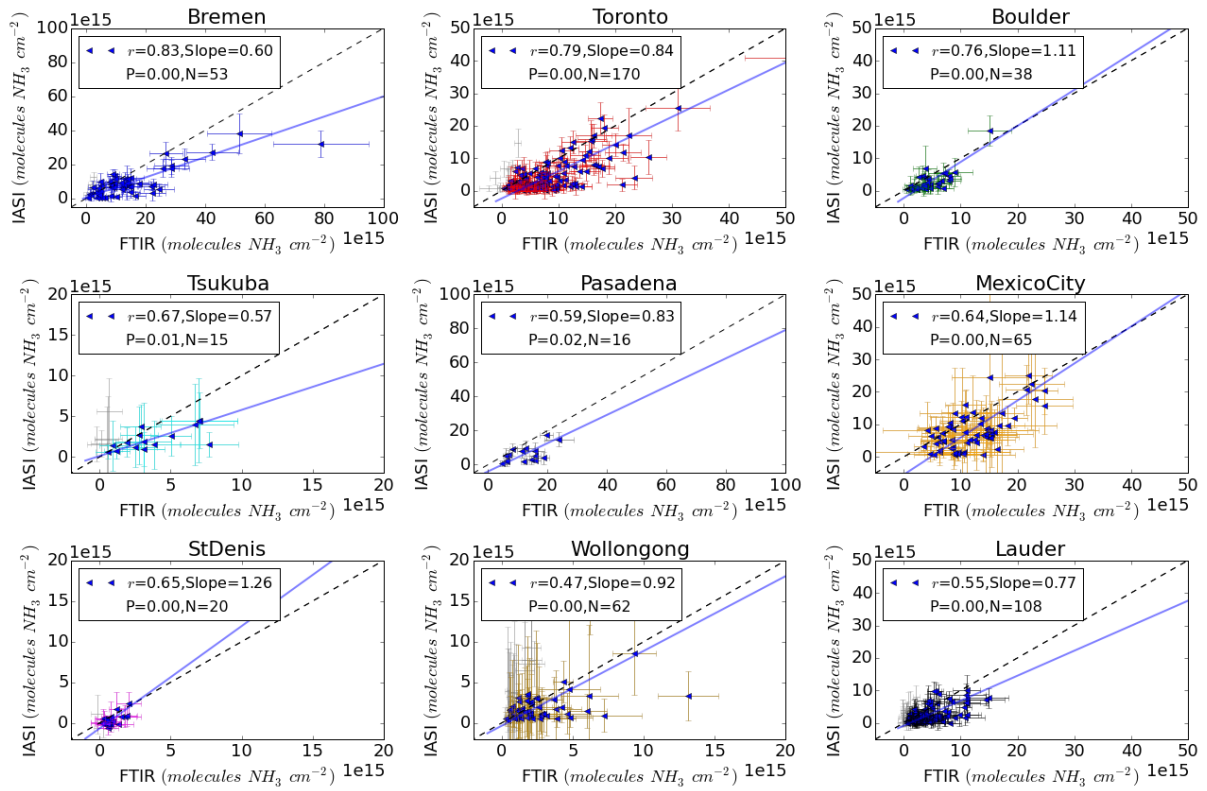


Figure 6. Correlations between the FTIR and IASI total columns with filters thermal contrast > 12, tdiff < 90min, xdifff < 25 km. The trend lines show the results of the regression analysis.

## Appendix A

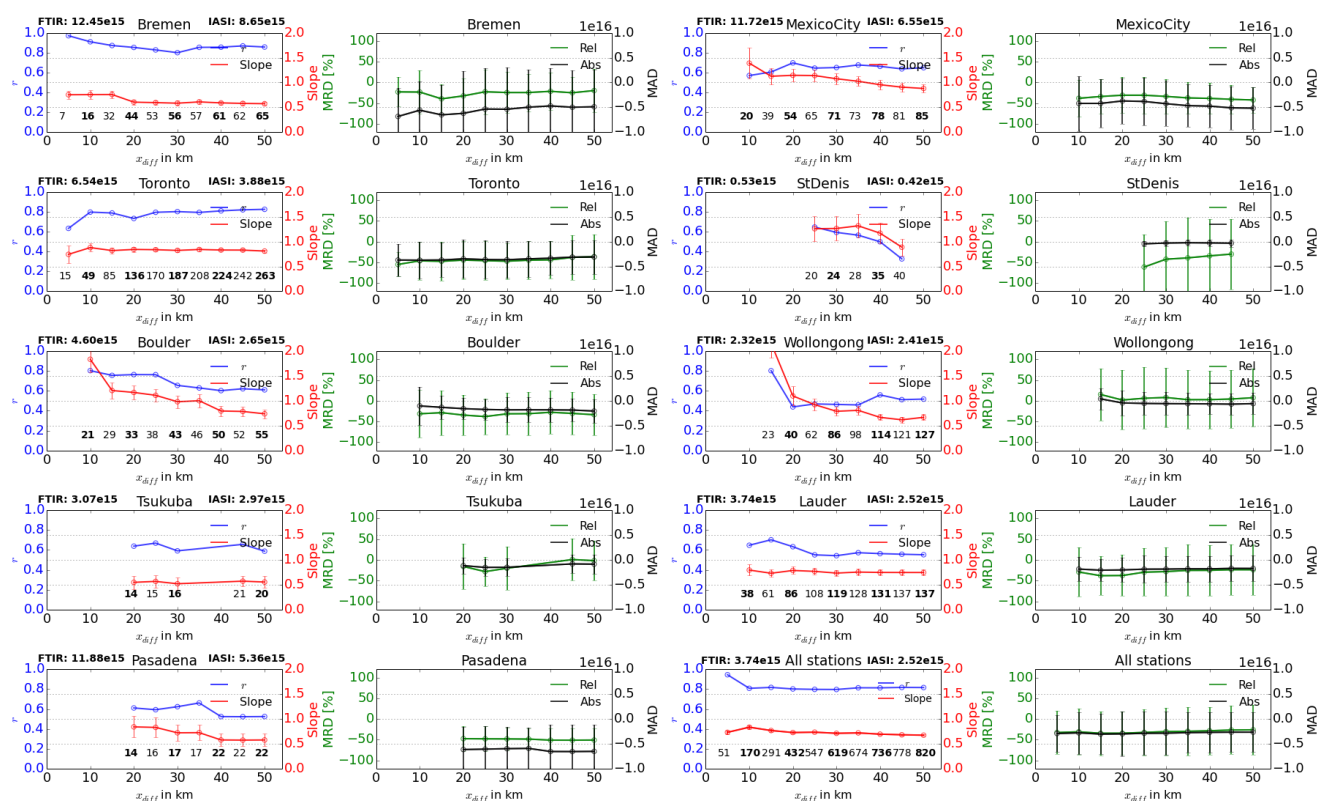


Figure A1. Correlation  $r$  (Blue lines, left figures), slope (Red lines, left figures) regression results, Mean Relative Difference (MRD, green lines, right figures) and Mean Absolute Difference (MAD, black lines, right figures) between IASI and FTIR observations as a function of  $x_{diff}$  for all sites. Bars indicate the standard deviation of the slope of the individual regression results. The numbers in the bottom of each subfigure show the number of matching observations. The numbers on the left and right side of the stations name give the mean FTIR and IASI total columns for a  $x_{diff} < 25$  km.

This section further covers the other stations, in addition to the sites covered by section 3.1.

The results for Mexico City show an overall constant correlation coefficient except for small criteria  $< 20$  km. The slope also decreases towards values seen at other stations. This effect could be due to a large number of sources inside the city, i.e. automobile and agricultural emissions in and near the city, increasing the heterogeneity of the found column totals. Reunion and Tsukuba have few coincident observations leading to only a few significant comparisons. This, combined with the low concentrations measured at Reunion leads to large differences in the mean and standard deviations of the subsequent  $x_{diff}$  sets. The Reunion and Wollongong observations are at the sensitivity limit of the IASI-NH<sub>3</sub> retrieval which limits the usefulness of the sites for the validation. As there are only a few observations for Tsukuba it is hard to make meaningful conclusions for the variability around the site.